Chiral [MnIIMnIII 3M'] (M'=NaI, CaII, MnII) and [MnIIMnIII 6NaI 2] Clusters Built from an Enantiomerically Pure Schiff Base: Synthetic, Chiroptical, and Magnetic Properties

Júlia Mayans,[a] Mercè Font-Bardia,[b] Lorenzo Di Bari,[c] Marcin Gjrecki,[c] and Albert Escuer*[a]

[a] J. Mayans, Prof. A. Escuer Departament de Qu&mica Inorg/nica i Org/nica Seccij Inorg/nica and Institut de NanociHncia i Nanotecnologia (IN2UB) Universitat de Barcelona, Mart& i Franques 1–11, Barcelona 08028 (Spain) E-mail: albert.escuer@qi.ub.es
Homepage: http://www.ub.edu/inorgani/recerca/MagMol/magmol.htm
[b] Dr. M. Font-Bardia Departament de Mineralogia, Cristal·lografia i Dipksits Minerals and Unitat de Difracció de R-X. Centre Científic i Tecnológic (CCiTUB) Universitat de Barcelona, Martí Franqués s/n, Barcelona 08028 (Spain)
[c] Prof. L. Di Bari, Dr. M. Górecki Dipartimento di Chimica e Chímica Industriale Università di Pisa, Via Moruzzi 13, 56124 Pisa (Italy)
and
Current address:
Institute of Organic Chemistry, Polish Academy of Sciences
Kasprzaka 44/52 St., 01-224 Warsaw (Poland)

ABSTRACT:

From the reaction of manganese halides with the chiral Schiff bases obtained by condensation of o-vanillin and (R)- or (S)-phenylglycinol, 11 complexes based on pentanuclear cages with trigonal bipyramidal [MnIIMnIII3M'] (M'=NaI, CaII, MnII) or enneanuclear [MnIIMnIII6NaI2] cores were synthesized. Structural, supramolecular chirality, and optical properties were explored. The magnetic properties of related systems were reviewed, and the magnetic response of the new systems was rationalized to the bond parameters.

Introduction

The characterization of the single-molecule magnet (SMM) response of anisotropic systems with high spin[1] or the modelization of the oxygen evolving center[2] (OEC) have been relevant driving forces of the research on polynuclear manganese clusters during the last two decades. Syntheses of cluster compounds often follow a serendipitous self-assembly process, but Schiff bases have attracted the attention of magnetochemists because of their polynucleating properties with the 3d transition of 4f lanthanide cations and because the adequate arrangement of the N- and O-donors, combined with the relative rigidity of the ligand, can allow predetermined shapes and/or nuclearities.

Condensation of o-vanillin and aminoalcohols yields multidentate Schiff bases for which a characteristic family of [MnIIMnIII 3Mn+] clusters with Mn+ =NaI and a trigonal bipyramidal arrangement of the cations has been reported,[3–10] together with a few examples in which Mn+ =Ca2+ or Ln3+.[3, 11] All of these clusters are characterized by the triangular arrangement of the trivalent manganese cations and the other two cations in apical positions resulting in a trigonal bipyramidal cage, in which the cations are held by three dianionic ligands.

Schiff bases derived from the condensation of 3-amino-1,2- propanediol with o-vanillin gives H3L ligands that satisfy all the coordination sites of the apical cations, which are hosted in two predetermined octahedral cavities[6–9] (Scheme 1-I). On the contrary, the H2L ligands derived from 2-amino-1-ethanol with only three O donors keep the octahedral cavity around the Na+ cation, whereas they generate an open face on the MnII cation[3–5, 10] that usually fulfills its coordination sphere with anions or solvent molecules (Scheme 1-II). In addition, this coordination gives the possibility to share the central cation or the open faces by means of bridging ligands that can join the pentanuclear units, resulting in larger nuclearities.[10, 12, 13] In these systems, the three ligands are parallel, and only one example with the divalent cation Ca2+ instead of Na+ has been reported as the OEC model[3] with one of the ligands inverted with respect to the other two (Scheme 1-III). A common point in these structures is the presence of three additional bridging ligands on the elongated coordination sites of the trivalent manganese cations. These co-ligands are usually carboxylates, halides, or pseudohalides (especially azide) in the search of ferromagnetic interactions and high-spin ground states.[14]

The employment of chiral 2-amino-1-ethanol aminoalcohols with substituents on the hydroxoethyl fragment generates chiral Schiff bases. Supramolecular chirality[15] is a growing field, which is of interest in chiral catalysis and Circular Polarized Luminescence (CPL) emission,[16] in the search for chiral magnets with d or f cations,[17, 18] or by its role in biological environments.[19] The synthesis of chiral clusters from enantiomerically pure ligands becomes of interest to reach multiproperty or multifunctional systems, in which optical, ferroelectric, or emissive properties can be combined with magnetic response. On the other hand, chiral clusters provide interesting examples of chirality transfer, chiral supramolecular arrangement, and chiral recognition.[20]

100   Following our work in this field[13], we chose the Schiff bases obtained from the condensation of o-

101   vanillin with (R)- or (S)-phenylglycinol (Scheme 2, top) to explore their reactivity in manganese

102   chemistry, with focus on the characterization of new chiral systems based on the [MnIIMnIII 3Mn+]

103   pentanuclear fragment. We report the characterization of 11 new chiral complexes with [MnIIMnIII

104   3NaI], [MnIIMnIII 3CaII], [MnII 2MnIII 3], and [MnIIMnIII 6NaI 2] nuclearity with formula

105   [Mn4NaOL3Br4]·[Mn4NaOL3Br4(H2O)]·[Mn4NaOL3Br3(MeOH)(MeCN)(H2O)]·[Mn4NaOL3Br3(

106   MeOH)(MeCN)2]Br2·6CH3CN·5CH3OH (1R) and

107   [Mn4NaOL3Br4(H2O)]·[Mn4NaOL3Br3(MeOH)(H2O)2]Br·6CH3CN· CH3OH (1S),

108   [Mn4CaOL3X5]·solvents (X=Cl, 2R and 2S; X=Br, 3S), [Mn5OL3X5]·solvents (X=Cl, 4R· and

109   4S·1.5MeCN; X=Br, 5S), and [Mn7Na2(O)2L6X6]·solvents (X=Cl, 6R and 6S; X=Br, 7R),

110   respectively. This series of compounds includes one enantiomeric pair of the chloro complexes for each

111   nuclearity (2R/2S, 4R/4S, and 6R/6S), and for comparative purposes, one example each of the

112   corresponding bromo derivatives (3S, 5S, and 7R). Structural trends and the confirmation of stability in

113   solution for complexes 1 and 6 were reported in a previous communication.[13b] The new systems were

114   structurally characterized and their chiroptical and magnetic properties studied pointing out the different

115   response of the types II and III (Scheme 1) classes of clusters. It is remarkable that compounds 2 and 3

116   with [MnIIMnIII 3CaII] nuclearity join the scarce number of similar complexes with this topology and

117   that the [MnII 2MnIII 3] and [MnIIMnIII 6NaI 2] nuclearities with trigonal bipyramidal or double

118   trigonal bipyramidal topology, respectively, are the first members of this family of complexes.

119

120

121

RESULTS AND DISCUSSION

Structural description

General trends

The reported complexes show some common features that will be described before the detailed comments of each structural type to avoid repetitive text. Several structures contain similar but nonequivalent molecules in the unit cell, and thus to simplify the discussion, all data in the main text are in relation to the "A" labeled molecule. All compounds possess a common core that can be described as a trigonal bipyramidal arrangement of three MnIII cations in the equatorial plane and two cations in the apical sites, resulting in the discrete [MnIIMnIII 3NaI] (1R, 1S), [MnIIMnIII 3CaII] (2R, 2S, 3S), [MnII 2MnIII 3] (4R, 4S, 5S), and the sharing vertex [MnIIMnIII 6NaI 2] (6R, 6S, 7R) metallic cores. In all cases, an oxo donor is placed in the center of the triangle determined by the MnIII ions with MnIII@O ond distances about 1.9 a. Also, two m-Cl (complexes 2, 4, and 6) or m-Br donors (complexes 1, 3, 5, and 7) are in all complexes and are coordinated in the elongated coordination sites of the trivalent manganese cations. Each pentanuclear unit is assembled by three Schiff bases in the deprotonated dianionic form, linking three different cations (Scheme 1-II and -III). The deprotonated O-alkoxo and O-phenoxo donors act as bridges between the equatorial cations and the cations in the apical sites. The oxidation state of the manganese cations was assigned according to the shape of the coordination polyhedral and bond valence sum (BSV) calculations (Table S1). The supramolecular aspects derived from the chiral character will be described for all compounds in the next section.

[Mn^{II}Mn^{III} $_3$Na^{I}] complexes 1R and 1S

Complexes 1R and 1S show the above described core with three L2@ ligands in the type-II molecular arrangement. The main bond parameters are summarized in Table 1, and a view of the pentanuclear unit is shown in Figure 1. O-phenoxide and O-alcoxide donors form a distorted octahedral pocket that hosts the NaI cation, which is linked to the three MnIII ions by means of NaI-Ophenoxide-MnIII bridges, whereas the linkage between the divalent and trivalent manganese ions is provided by three MnII-Oalcoxide-MnIII bridges. In the center of the equatorial plane, one m4-O ligand links the three MnIII cations and the NaI cation. This oxo donor is slightly shifted from the center of the triangle toward the NaI cation, which can be assumed as heptacoordinated. Three faccoordination sites of the divalent manganese cation are occupied by three O-alkoxo donors, but the remaining coordination sites are fulfilled in multiple forms that differ in the coordination of the MnII cation. Structure 1R contains four non-equivalent clusters that contain one tetrahedral Mn4A cation (MnO3Br environment), two hexacoordinated Mn4B and Mn4C cations (MnO5N and MnO4N2 environments, respectively), and one pentacoordinated Mn4D (MnO4Br environment). Complex 1S also exhibits two nonequivalent units

with Mn4A and Mn4B in MnO4Br and MnO6 coordination environments, respectively. Consequently, MnIII-O-MnII bond angles show characteristic values as a function of the Mn4 coordination number, which are close to 1228 (octahedral MnII), 1188 (pentacoordinated MnII), and 1118 (tetrahedral MnII) (Figure 1 and Table 1).

Units 1RA, 1RD, and 1SA are neutral but 1RB, 1RC, and 1SB are cationic, and thus, the charge balance is fulfilled with two (1R) or one (1S) Br@ counteranion.

Compounds 1R and 1S are not enantiomers in a strict sense because they crystallize in different space groups (P1 and P21, respectively), but on the other hand, cell parameters, bond parameters for the cage, and its helicity follow the similitude or mirror image that must be expected for a normal pair of enantiomers. These differences are due to the plasticity of the MnII coordination sphere, which links different solvents or Br@ ligands and is limited to the Mn4 environment.

$[Mn^{II}Mn^{III}{}_3Ca^{II}]$ complexes 2R, 2S, and 3S

Complexes 2R, 2S, and 3S show the trigonal bipyramidal metallic core described above with three MnIII cations in the equatorial plane, however for these compounds, the apical sites are occupied by one MnII and one CaII cation (Figure 2). The main bond parameters are collected in Table 2. The three structures contain two nonequivalent clusters, but in this case, there are only minor differences between them. The main difference with the previously described complexes consists in the reversed coordination of one of the ligands and the concomitant loss of the C3 symmetry (type-III arrangement in Scheme 1). As in the previous case, the oxo donor placed in the center of the triangle defined by the three MnIII cations is also shifted toward the CaII ion, which is assumed to be heptacoordinated, and then the O donor is a m4-O ligand. The environment of Mn4 is defined by two O-alkoxo donors, one phenoxo/methoxide bidentate group, one solvent molecule, and one chloro donor, whereas the environment for Ca1 is defined by two phenoxo/methoxide bidentate groups, one O-alkoxo donor, one coordinated chloro ligand, and contact with the m4-O donor resulting in neutral clusters in all the cases. The important asymmetry derived from the 2:1 reversed Schiff bases is translated to the MnII-O-MnIII bond angles which show significant differences with respect to complexes 1R and 1S; the MnII-Oalkoxo-MnIII bond angles are larger than the MnII-Ophenoxo- MnIII bond angles. In the same way, the MnIII 3 triangle becomes scalene. The main intermolecular contacts consist of weak CH···Cl hydrogen bonds involving the chloro ligands coordinated to the MnII cations.

$[Mn^{II}{}_2Mn^{III}{}_3]$ complexes 4R, 4S, and 5S

The neutral complexes 4 and 5 show the same structure as that of the analogous 2 and 3 complexes but with one MnII cation in the position that was occupied before by the calcium ion (Figure 3). In contrast with the CaII analogues, the oxo donor is centered in the MnIII 3 plane and should be assumed strictly as a m3-O ligand. The coordination of the cations and the intermolecular contacts are very similar to

194   those of the isostructural CaII complexes. The two MnII cations show an octahedral MnO5X (X = Cl,

195   Br) environment but are not equivalent because Mn4 links two O-alkoxo donors and one Ophenoxo

196   donor, whereas Mn5 links one O-alkoxo and two Ophenoxo donors with the consequent asymmetry and

197   different MnIII-O-MnII bond angles as a function of each kind of bridge (Table 3).

198

199   ## [Mn^{II}Mn$^{III}_6$Na$^I_2$] complexes 6R, 6S, and 7R

200   The nonanuclear [MnIIMnIII 6NaI2] core of the (R) and (S) pair of enantiomers of 6 consists of two

201   pentanuclear units (similar to those described for complex 1) sharing the octahedral MnII cation (Figure

202   4). The main bond parameters are summarized in Table 4.The 22 positive charges are balanced by the

203   six dianionic Schiff bases, two m3-oxo donors, and six m-Cl bridges in the axial coordination sites of

204   the MnIII cations. The L2@ ligands and the MnIII cations in each pentanuclear subunit are related by

205   one C3 axis (R3 space group), but the lack of inversion center between them determines different bond

206   parameters around the divalent Mn3 in each subunit; the Mn2-O4-Mn3 bond angle takes a mean value

207   of 125.8(3)8, whereas the mean bond angle for Mn1-O1-Mn3 is 122.9(3)8. Complex 7R exhibits the

208   same core and similar bond parameters to those of complex 6, except for the logically larger MnIII@Br

209   bonds. However, in this case the complex crystallizes in the triclinic P1¯ space group, the C3 symmetry

210   is lost, and the MnIII-O-MnIII bond angles are slightly different, ranging be- tween 117.3–120.38. The

211   main bond parameters and a labelled plot are shown in Table S2 and Figure S1, respectively.

212   Notably, in all cases the oxo ligands are slightly shifted out of the MnIII 3 plane toward the NaI cation,

213   with Na@O bond distances of about 2.7 a, and thus, the coordination of the sodium ions can be formally

214   described as an apicated octahedron, and the oxo donors can be assumed as m4-O ligands.

215

216   **Chirality transfer**

217   The employment of enantiopure chiral ligands determines the configuration of the derived complexes.

218   Chirality can be transferred to the environment of the cations, to the overall complex or even to the

219   crystalline network. This "predetermined chirality" is propagated in the opposite sense by the

220   corresponding enantiomeric ligands, resulting in mirror-image clusters or networks.[15] The reported

221   complexes offer a variety of situations, from the conventional chirality transfer to some unusual

222   responses.

223   For compounds 1R and 1S, the L2@ ligands are tilted in the same sense with respect to the main axis of

224   the complex, and thus, the whole molecule shows a helical arrangement that turns in opposite sense for

225   each cluster (L for 1R and D for 1S), as shown in Figure 5. Locally, the environment of the manganese

226   cations is not chiral but the tris-bidentate donors around the NaI cation define a propeller shape, with

227   chirality also L for 1R and D for 1S. In this case, the different orientation in the network of the

228   nonequivalent molecules does not transfer the chirality to the network.

229   The related complexes 2–5 also show a helical arrangement of the Schiff bases, but surprisingly, the

230   helicity of the two parallel ligands turns in opposite sense with respect to the reversed ligand, and thus,

231   the propeller shape of the cluster is not achieved.

232   The two nonequivalent molecules in the network also turn in opposite sense to one another, that is, the

233   parallel ligands in molecule A turn D and the reversed ligand turns L, whereas for the molecule labeled

234   B, these ligands turn L and D, respectively (Figure 6). As a direct consequence, the cations linked to

235   three bidentate fragments (CaII for 2 and 3 or one of the MnII cations for 4 and 5) also show opposite

236   conformation that cannot be classified as purely L or D. The reason for this highly unusual feature can

237   be found in the packing of the clusters, which show a parallel arrangement in the cell with the

238   nonequivalent units rotated 1808 relative to each other. This arrangement shows an equivalent

239   distribution of the pending phenyl groups at each side of the molecules, probably favouring a most

240   effective packing of the clusters. This structure is ex tremely unusual because the presence of two quasi

241   mirrorimage molecules in the same cell for a chiral system means that there is a poor chiral induction

242   from the ligand onto the system. This configuration has been observed only once for the related CaII

243   complex reported by Powell et al.[3]

244   Finally, complexes 6 and 7 also offer an unusual feature: in this case, the three ligands are parallel,

245   similar to that which occurs in complexes 1R and 1S, and thus, the [MnIIMnIII 3NaI] subunits show the

246   expected propeller shape but the two fragments turn in the opposite sense, and consequently, the tris-

247   bidentate environment of the Na1 and Na2 cations of the same cluster show opposite D and L

248   configurations. However, some degree of transference of chirality arises from the central MnII cation,

249   which is slightly distorted from Oh symmetry to trigonal prism, and this trigonal rotation is transferred

250   to the two moieties of the molecule, breaking a strict regular alternate shape for the two [Mn3OCl3]

251   triangular planes. This rotation takes place in the opposite sense for each enantiomer, as well as in the

252   arrangement of the phenyl groups in the molecular shell, which also show a mirror image between them

253   (Figure 7).

254

255   **Comments on the syntheses**

256   The reaction of the Schiff base H2L with manganese halides and further air oxidation led to the

257   formation of [MnIIMnIIIM'] mixed-valent pentanuclear cages with trigonal bipyramidal shapes.

258   Notably, the syntheses of isolated or fused cages or the nature of M' is related to the reaction conditions

259   (Scheme 3). Reaction of manganese bromide with the (R)- or (S)-H2L ligand in the presence of sodium

260   azide allowed the crystallization of compounds 1R and 1S, which contain m-Br donors in the elongated

261   coordination sites of the MnIII cations and one MnII and one NaI cation in the apical sites of the core. In

262   this reaction, the azide anion is not coordinated, and its role is then limited to provide basic medium and

263   to contribute to deprotonation of the organic ligand. However, the base is not innocent because complex

264   7R, which consists of two pentanuclear units sharing the MnII cation, was obtained when sodium

265 hydroxide was employed instead of sodium azide. In contrast, when manganese chloride was employed
266 as the starting salt, only the nonanuclear [MnIIMnIII6NaI2] cages were obtained in all cases.
267 In these cages with the [MnIIMnIII3NaI] core, the sodium cation is placed in a NaO6 cavity determined
268 by the bidentate phenoxo/methoxide fragments of the ligands. This cavity seems a priori quite flexible,
269 and thus, the reaction with larger cations such as KI or CsI was tried by employing the corresponding
270 hydroxides to deprotonate the ligands. The result of this reaction, independent of the starting manganese
271 halide, was the characterization for the first time of the related pentanuclear [MnII2MnIII3] systems
272 (complexes 4R, 4S, 5S). This fact proves that the size of the O6 pocket is selective for sodium cations
273 and that the system prefers the coordination of a second MnII cation instead of the larger alkaline ions.
274 Given that the size of the cations plays a determinant role in the conformation of the final cage, the CaII
275 cation, which has a similar ionic radius to that of NaI (close to 1 a in a hexacoordinated environment),
276 was selected to attempt the characterization of new [MnIIMnIII3CaII] cages. The employment of
277 calcium methoxide as a base to deprotonate the organic ligands led effectively to the desired core in
278 complexes 2R, 2S, and 3S.
279 When the cavity is occupied by NaI, the three Schiff bases exhibit a parallel arrangement along the main
280 axis of the molecule. However, the substitution by a divalent cation induces the antiparallel coordination
281 of one of the ligands, in agreement with the same type-II ligand arrangement reported by Powell et al.[3]
282 for a related cage containing the calcium cation instead of sodium.
283 All samples were prepared at room temperature, and during the different syntheses, we realized that they
284 were poorly sensitive to changes in the manganese/ligand ratio and to the source of basic medium if
285 alkaline ions were present. The complexes are stable at room temperature in the mother solution for
286 weeks.
287
288 **UV/Vis and ECD spectroscopy**
289 Tong et al.[4] previously reported the UV/Vis and electronic circular dichroism (ECD) spectra for the
290 H2L ligand; the absorptions in the UV region were assigned to the transitions of the aromatic groups (p–
291 p*) of the Schiff base, and the less intense band at about 400 nm was assigned to the n–p* transition of
292 the azomethine chromophore. As expected, the UV/Vis spectra for 1–7 show common absorptions for
293 all complexes that are attributable to ligand transitions (Figure S2).
294 ECD spectra confirm the enantiomeric nature of the reported systems, with mirror images of the spectra
295 for all the reported pairs of clusters. Complexes 1–7 exhibit several structural variables such as the choro
296 or bromo donors at the axial coordination sites of the MnIII cations, different cations in one of the core
297 sites (NaI, CaII, or MnII) or different nuclearity (complexes 6 and 7). To elucidate the factors that can
298 influence the resulting spectra, an inspection of the shape of the spectra evidences a clear similitude
299 between the plots for the 1 and 6 pairs of enantiomers, which show a practically identical distribution of
300 absorptions and intensities in the 275–800 nm range (with a minor difference in the intensity of the 275
301 nm band) and a different response for complexes 2 and 4, which show an intense transition centered at

302 400 nm and apparently no features above 450 nm (Figure 8). These data indicate that halide or cation

303 substitutions are irrelevant and that the main differences in the ECD spectra must be related to the

304 relative position of the ligands for 1, 6, and 7 compared to that of 2–5. This assumption is reinforced by

305 the perfect agreement between the spectra of complexes 2 and 4 which contain two very electronically

306 different cations such as CaII or MnII, suggesting that the weak absorptions at larger wavelengths

307 involves transitions between the iminic fragments and the MnIII cations.

308 It becomes relevant that the EDC spectra can unambiguously differentiate the type-II and III topologies

309 (Scheme 1), and thus, provide a new example of the application of this technique to obtain structural

310 information of complexes in solution.

311

Magnetic properties

313 The magnetic properties for complexes 1–7 were measured for powdered samples in the 2–300K

314 temperature range. The high number of superexchange pathways (from 6 for 1 to 12 for 6–7), the zero

315 field splitting (D) of the anisotropic MnIII cations, and the intermolecular interactions imply a large

316 number of variables that, unless the symmetry is simplified, bring overparametrized Hamiltonians.

317 Therefore, the fit of the experimental data requires rational criteria to employ simplified Hamiltonians to

318 extract significant information about the values of the J coupling constants and to rationalize the

319 magnetic response.

320 The interaction between the apical MnII cation and each MnIII cation is mediated by a single MnII-

321 Oalkoxide-MnIII bridge that gives antiferromagnetic interactions in this type of cluster. The MnIII

322 cations are held together by one m3-O bridge with short MnIII@O bond distances and additional m2

323 ligands that link the coordination sites on the elongated Jahn–Teller axis. Thus, the interaction between

324 these cations seems apparently mediated by the main superexchange MnIII-O-MnIII pathway, for which

325 previous studies have shown that the ferromagnetic-antiferromagnetic (FM/AF) limit for a [MnIII3(m3-

326 O)] fragment is found around the 1208 MnIII-O-MnIII bond angle and that the shift of the central m3-O

327 from the Mn3 plane favors the ferromagnetic interactions.[21, 22] The assumption of one AF interaction

328 between the MnII and the MnIII cations and the FM/AF bond-angle dependence of the interaction

329 between the MnIII cations has been systematically applied as general criterion to rationalize the

330 magnetic properties of [MnIIMnIII3M’] systems,[3–10] although these correlations were performed for

331 MnIII triangles with the elongated axis perpendicular to the MnIII3 plane and with m2 ligands (oximate

332 and others) in the triangular edges which strongly contribute to the superexchange mechanism.

333 Preliminary attempts to fit the reported systems applying this usual criterion were satisfactory for

334 complex 1 but were unable to adequately reproduce the experimental data for the new topologies of 2–7.

335 To check the commonly accepted explanation of the magnetic response of these systems, we reviewed

336 and analysed the main bond and magnetic parameters for the 12 [MnIIMnIII3Na] complexes reported up

337 until now; this is summarized in Table 5 (see also Scheme 4). A simple inspection of the reported data

338 points out several facts: 1) the MnII-O-MnIII interaction is effectively antiferromagnetic in all cases; 2)

the shift of the m3-O donor from the Mn3 plane is very similar in all cases, and thus, its influence is not a relevant variable; 3) often the systems have low symmetry due to the m2 additional ligands that, in some cases, induces large deviations from 1208 for the MnIII-O-MnIII bond angle (usually lower than 1208 for monoatomic bridges such as Cl@, m1,1-N3, etc. or much larger than 1208 for syn-syn carboxylates or m1,3-N3).

Surprisingly, it becomes evident that there is a complete dispersion of J values versus the MnIII-O-MnIII bond angle (Figure S3) and that very different J values have been reported for the same m2 ligand and bond angle as is the case for the m2-Cl ligand (LIQXOA compared with WIMBIF) or the pairs of complexes with m1,1-N3, m1,1-N3, m1,3-N3 m2 ligands (XIJMAG compared with RILZAP) and the pair of complexes with H2O, H2O, PhCOO@ ligands (XIJMIO compared with RILZUJ), as shown in Table 5.

We also realized that some fits were poorly reliable because they were unable to reproduce the full experimental susceptibility plots and were performed with the discarding of data below 25–50 K. This lack of correlation points out that the problem is more complex and cannot be reduced to a simple correlation with the MnIII-O-MnIII parameter and also that the contribution of the m2-ligand pathway and the differentiation of different values for the MnII-O-MnIII interactions cannot be discarded. Considering these features and taking into account that in our case the contribution of the m2-Cl additional ligands is constant for all complexes, our procedure was: 1) to employ isotropic Hamiltonians, to employ a zJ parameter for the low T deviations to reduce computational requirements in the cMT fits, and to take into account the D effect in the more sensitive magnetization simulations; 2) to join under the same J parameter the pathways mediated by the same kind of bridges independently of slight differences in the bond parameters. This means to assume one common J1 coupling constant between MnIII-MnIII cations inside the m3-O centered triangles, one common J2 coupling constant between MnIII-MnII cations linked by O-alkoxo bridges, and a different J3 coupling constant between MnIII-MnII cations linked by O-phenoxo bridges in the case of compounds 2–5.

On the basis of the above considerations, the interactions can be described as is shown in Scheme 5. As is expected from the structural data, the magnetic behaviour of the reported complexes is similar for each core, independently of the chirality of the Schiff base, and thus, one example of each core and bridging halide placed in the axial coordination sites of the MnIII cations will be discussed.

The room-temperature cMT value for complex 1S is 10.5 cm3mol@1 K, lower than the value expected for three MnIII and one MnII isolated cation (13.375 cm3mol@1K for g=2.00). On cooling, cMT decreases continuously down to a plateau between 25–5 K and finally decreases slightly at lower temperatures, reaching a value of 6.2 cm3mol@1K at 2 K (Figure 9). Assuming a common J constant for each MnIII-MnIII or MnIII-MnII pathway, and according to Scheme 5, the two-J Hamiltonian is given by Equation (1):

$$H = -2J_1(S_1 \cdot S_2 + S_2 \cdot S_3 + S_1 \cdot S_3) - 2J_2(S_1 \cdot S_4 + S_2 \cdot S_4 + S_3 \cdot S_4) \tag{1}$$

Fit of the experimental data gave an excellent fit for J1=0.96 cm@1, J2=@3.1 cm@1, g=1.86, and R=1.3V10@5 (corrected with a zJ=@0.005 cm@1 for the low T decay). The calculated energy of the spin levels shows a well-isolated S=7/2 ground state with a gap of 27 cm@1 to the first S=9/2 excited state. This ground state, which comes from the antiferromagnetic interaction of the MnII (S=5/2) with the local S=6 from the MnIII3 triangle, is confirmed by the magnetization measurement that tends to an unsaturated value of 5.7 NmB under the maximum applied field of 5 T, in agreement with data reported for related [MnIIMnIII3Na] systems with ST=7/2.[8, 10] This value is close to that expected for seven electrons, assuming the calculated g value from the susceptibility fit (6.5 NmB). The difference must be attributed to a D effect, and the fit of the magnetization data as an isolated 7/2 spin was satisfactory for a D value of @0.4 cm@1 (inset of Figure 9).

Room-temperature cMT values for complexes 2R and 3S are 12.4 and 12.7 cm3mol@1 K, respectively. On cooling, cMT decreases down to well-defined minimums at 12 K (8.9 cm3mol@1K for 2R and 9.0 cm3mol@1K for 3S). Below the minimum, cMT increases to reach 10.2 cm3mol@1K for 2R and 11.2 cm3mol@1K for 3S at 2 K (Figure 10).

The core of complexes 2R and 3S is similar to that of the above described complexes 1R and 1S, but in this case, the system is fully asymmetric due to the antiparallel orientation of one of the Schiff bases. The MnIII-O-MnIII bond angles are slightly different, and there are two alkoxo and one phenoxo MnIII-O-MnII bridge. Assuming one J coupling constant for each kind of superexchange pathway, and according to Scheme 5, the resulting 3J-Hamiltonian is given by Equation (2):

$$H = -2J_1(S_1 \cdot S_2 + S_2 \cdot S_3 + S_1 \cdot S_3) - 2J_2(S_1 \cdot S_4 + S_3 \cdot S_4) - 2J_3(S_2 \cdot S_4) \tag{2}$$

Fit of the experimental data in the full temperature range of 2–300K was satisfactory for J1=@2.7 cm@1, J2=2.1 cm@1, J3=@1.8 cm@1, g=1.94, and R=8.1V10@5 for 2R and J1=@1.1 cm@1, J2=1.3 cm@1, J3=@3.4 cm@1, g=1.97, and R=8.2V 10@5 for 3S. A simple analysis of the shape of these plots evidence the following facts. First, the increase of cMT at low temperature discards a response similar to that of complex 1S because for a ferromagnetic MnIII3 triangle (local S=6) interacting with one MnII cation, only monotonically increasing or decreasing plots tending to S=17/2 or 7/2 should be expected (S=6:5/2 possible ground levels). Second, the cMT increase at low temperature suggests that low-lying S levels with larger spin must be very close to the S ground state. Calculation of the energy of the S levels for the calculated J values shows two quasi-degenerated ground spin levels S=7/2 and S=9/2

413   that are highly populated at 2 K (49.8% and 49.3 %, respectively, for 2R and 24.9% and 73.1 %,

414   respectively, for 3S, Table S3). The population of the larger spin level determines the increase of cMT at

415   low temperatures, and in fact, the experimental cMT values at 2 K are intermediate between 7.875

416   cm3mol@1K (S=7/2) and 12.375 cm3mol@1K (S=9/2). Magnetization experiments reveal unsaturated

417   plots tending to 6.21 and 6.72 NmB for 2R and 3S, respectively, under the maximum explored field of 5

418   T (inset of Figure 10). The similar and close S levels in the vicinity of the ground state exclude the

419   accurate fit of the magnetization. In this case, there is only one similar complex reported by Powell et

420   al.,[3] with m1,1-N3 and m1,3-N3 bridges, which shows an S=1/2 ground state that was related to the

421   AF interaction attributed to the end-to-end azido bridge and the large MnIII-O-MnIII angle. Trials to fit

422   the systems by adding different superexchange parameters for the different MnIII-OMnIII bond angles

423   did not improve the quality of the fits.

424   The cMT plots for complexes 4R and 5S show very similar room-temperature values of 16.0 and 15.8

425   cm3mol@1 K, close to the expected cMT value for three MnIII and two MnII isolated cations (17.75

426   cm3mol@1K for g=2.00). On cooling, cMT decreases continuously down to 2.7 and 3.9 cm3mol@1K

427   for 4R and 5S, respectively (Figure 10). According to the low symmetry and alkoxo/phenoxo

428   distribution of the MnIII-O-MnII bridges, the proposed Hamiltonian based on Scheme 5 is given by

429   Equation (3):

430

431

432    $$H = -2J_1(S_1 \cdot S_2 + S_2 \cdot S_3 + S_1 \cdot S_3) - 2J_2(S_1 \cdot S_4 + S_3 \cdot S_4 + S_2 \cdot S_5) - 2J_3(S_2 \cdot S_4 + S_1 \cdot S_5 + S_3 \cdot S_5)$$ (3)

433

434

435   Best fit of the experimental data was obtained for J1=@1.7 cm@1, J2=@0.57 cm@1, J3=@1.2 cm@1,

436   g=1.96, and R=8.7V10@6 for 4R and J1=@1.6 cm@1, J2=@1.0 cm@1, J3=@0.82 cm@1, g=1.96, and

437   R=1.8V10@5 for 5S. As a consequence of the competitive interactions in all the triangular faces of the

438   core of these complexes, the ground state becomes not evident. The calculation of the energy of the S

439   states shows an S=2 ground state for these two compounds but with several very close S=1, S=2, and

440   S=3 spin levels. As a function of their population, the cMT value at 2 K is closer to an S=2 for 4R or

441   intermediate between S=2 and S=3 for 5S (Table S3). In agreement, the magnetization plots show a

442   continuous increase that corresponds to the population of larger S levels under higher fields (inset of

443   Figure 10), reaching the unsaturated values of 5.61 and 4.46 NmB for 4R and 5S, respectively. The large

444   number of close spin levels exclude the fit of the magnetization. Trials to fit the systems by adding

445   different superexchange parameters for the different MnIII-O-MnIII bond angles did not improve the

446   quality of the fits.

447   The cMT plots for complexes 6R and 7R show, as in the previous cases, similar response for the m-

448   chloro or m-bromo complexes. The room-temperature cMT values of 19.3 and 17.9 cm3mol@1K for 6R

449   and 7R, respectively, are close to the expected values for six MnIII and one MnII noninteracting cation

450   of 22.375 cm3mol@1K (g=2.00). On cooling, cMT decreases down to a well-defined minimum around

451   110 K, followed by an increase up to 27.7 cm3mol@1K (6R) or 26.7 cm3mol@1K (7R) at 13 K. At

452   lower temperature, the cMT plot decreases to reach values around 22 cm3mol@1K (Figure 11).

453   Complex 6R possesses one C3 axis, and consequently, all the MnIII-MnIII or MnIII-MnII pathways are

454   strictly equivalent by symmetry, and the system can be simulated with only two coupling constants, J1,

455   joining all the MnIII···MnIII interactions and J2, joining all the MnII···MnIII interactions. The same

456   coupling scheme was applied to compound 7R. The applied two-J Hamiltonian is given by Equation (4):

457

458    $H = -2J_1(S_1 \cdot S_2 + S_2 \cdot S_3 + S_1 \cdot S_3 + S_4 \cdot S_5 + S_4 \cdot S_6 + S_5 \cdot S_6) -$ (4)

459    $2J_2(S_1 \cdot S_7 + S_2 \cdot S_7 + S_3 \cdot S_7 + S_4 \cdot S_7 + S_5 \cdot S_7 + S_6 \cdot S_7)$

460

461   Fitting by employing the above Hamiltonian and taking into account the zJ parameter to include the

462   decay of cMT below 15K was unable to correctly reproduce the low T region, and thus, the isotropic fit

463   was performed in the 25–300 K range. Best fit parameters for these limited fits were J1=1.65 cm@1,

464   J2=@2.85 cm@1, g=1.96, and R=4.2V10@5 for 6R and J1=0.77 cm@1, J2=@3.74 cm@1, g=1.96, and

465   R=5.2V10@5 for 7R.

466   Magnetization experiments show a continuous increase in the magnetization, reaching the unsaturated

467   values of 11.95 and 12.21 NmB for 7R and 6R, respectively. These values are far from the expected

468   values corresponding to the ground state S=19/2 derived from the antiferromagnetic interaction of the

469   central S=5/2 ion with two ferromagnetic MnIII triangles with S=6 local spins. Surprisingly, the fit of

470   the experimental data as isolated spins is satisfactory for a S=15/2, D=0.2, and g=1.83 for 6R and

471   S=13/2, D=0.3, and g=1.87 for 7R, which seems to be not compatible with the values derived from the

472   susceptibility data. Considering the lack of consistence of the magnetization and the difficulties to fit the

473   low-temperature cMT data, and that any other simplification cannot be proposed because of the strict C3

474   symmetry of the complexes, we decided to explore the effect of the interaction between the two

475   ferromagnetic triangles through the MnII cation in a similar manner to the typical interaction between

476   the peripheral cations in a simple linear trinuclear system, which in this case is equivalent to a S=5/2

477   central ion and two peripheral S=6fragments.

478   The inclusion of the interactions between the MnIII cations of the two triangles revealed to be extremely

479   important, and as can be seen in Figure 12, the S=19/2 spin level remains the ground state until an

480   interaction value close to @0.5 cm@1, however, for larger AF interactions, the ground state changes

481   quickly to lower values.

482   In the same way, low-temperature cMT decreases and the magnetization strongly decreases when the

483   S=19/2 and 17/2 spin levels increase in energy.

484   In light of these calculations, a new fit including the intertriangle interaction for the J value

485   corresponding to the ground state suggested by the fit of the magnetization yield is an excellent fit for

486   the whole range of temperatures for an intertriangle interaction of @0.7 cm@1 and J1=3.3 cm@1,

J2=@3.4 cm@1, g=1.84, and R=8.8V10@5 for 6R and an intertriangle interaction of @0.75 and J1=3.3

cm@1, J2=@3.2 cm@1, g=1.90, and R=2.0V10@4 for 7R.

Absolute J and g values for this system must be assumed with caution because of the number of superexchange parameters, but independently of the fit approach, the sign of the interactions is always AF between MnII···MnIII and FM inside the triangular MnIII unit. Complexes 6R and 7R can be envisaged as two fused [MnIIMnIII3NaI] fragments with similar C3 symmetry and bond parameters, and as should be expected, the sign of the coupling constants is the same as that in compound 1 and the two complexes with m2-Cl bridges reported in the literature.[8, 13]

Alternate current measurements were performed for all the complexes, but no out-of-phase signals were observed either at zero field or under static fields, discarding a SMM response, probably as a result of the sum of several factors such as the unfavorable arrangement of the easy axis of the MnIII cations, low D values, or the mixing of multiple spin states in the vicinity of the ground state that provide fast relaxation.

The magnetic response of the reported systems and the successful rationalization of their magnetic response provide some conclusions: first, in this case, the m2-ligands (Cl or Br) have a negligible influence on the magnetic properties, and second, the generally assumed criterion to justify the magnetic response of related complexes is dubious. The magnetic properties of these systems can be explained without the employment of different J constants for different MnIII-O-MnIII bond angles for a constant m2 ligand.

CONCLUSION

The chiral Schiff base derived from the condensation of o-vanillin and phenylglycinol proved to be a versatile ligand that, in adequate experimental conditions, is able to generate a variety of nuclearities and conformations based on the pentanuclear fragment [MnIIMnIII3M'(m3-O)2L3]. New examples of the M'=NaI family, some rare M'=CaII complexes, and the first clusters with M'=MnII or the enneanuclear systems [MnIIMnIII6NaI2(m3-O)2L3] were characterized. ECD and IR spectroscopy proved to be able to differentiate the parallel or reversed arrangement of the ligands, with the latter related to the inclusion of divalent cations in the M' position. The reversed arrangement is associated with the anomalous loss of molecular helicity for both enantiomers. A review of the previously published data for the [MnIIMnIII3NaI] family of clusters revealed that the usually accepted dependence of the MnIII-O-MnIII bond angle of the triangular fragments is poorly reliable to analyze their magnetic properties and that the superexchange role of the axial ligands must be considered.

EXPERIMENTAL SECTION

Experimental details

IR spectra (4000–400 cm@1) were recorded with a Bruker IFS-125 FTIR spectrometer with samples prepared as KBr pellets. Variabletemperature magnetic studies were performed with a MPMS-5 Quantum Design magnetometer operating at 0.03 T in the 300–2.0 K range. Diamagnetic corrections were applied to the observed paramagnetic susceptibility using Pascal's constants. Analysis of the magnetic data was performed with the PHI program.[23] Quality of the fits was parametrized as the R=(cMTexptl @cMTcalcd)2/(cMTexptl)2 factor.

The solution ECD and UV/Vis spectra were recorded with a Jasco J-715 spectrometer at RT in spectroscopic grade CH3CN (10@5m, compounds 1 and 6) or CH3OH (10@6m, compounds 2 and 4). The solutions were measured in quartz cells with a path length between 2 and 0.1 cm. All spectra were recorded by using a scanning speed of 100 nmmin@1, a step size of 0.1 nm, a bandwidth of 2 nm, a response time of 0.5 s, and averaged over four accumulations. The spectra were baseline-corrected by using the solvent spectrum under the same conditions and immediately before or after the sample measurement. For all compounds, the yields of the syntheses were about 30–40% of crystalline product that was employed for the instrumental measurements.

Single-crystal X-ray crystallography

Prismlike specimens of the 11 (R) and (S) enantiomers of 1–7 were used for the X-ray crystallographic analyses. The X-ray intensity data were measured with a D8-VENTURE system equipped with a multilayer monochromator and a Mo microfocus (l=0.71073 a). The frames were integrated with the Bruker SAINT software package using a narrow-frame algorithm. The final cell constants were based upon the refinement of the XYZ-centroids of reflections above 20 s(I). Data were corrected for absorption effects using the multi-scan method (SADABS). The structures were solved with the Bruker SHELXTL Software Package and refined using SHELXL.[24] Details of crystal data, collection, and refinement for 1R and 1S are summarized in Table S4, 2R, 2S, and 3S in Table S5, 4R, 4S, and 5S in Table S6, and 6R, 6S, and 7R in Table S7. Analyses of the structures and plots for publication were performed with Ortep3[25] and POVRAY programs.

Synthetic procedures

H2L Schiff bases: The corresponding (R)- or (S)-enantiomer of 2-phenylglycinol (0.5 g, 3.64 mmol) and 2-hydroxy-3-methoxybenzaldehyde (0.55 g, 3.64 mmol) were dissolved in methanol (20 mL), and the solution was refluxed for 1 h and diluted to 50 mL with methanol. The resulting 0.072m yellow solutions of the H2L ligands were employed directly in the synthesis of the derived complexes.

Complexes with [Mn4Na] core (1R and 1S): MnBr2·4H2O (0.104 g, 0.365 mmol) and NaN3 (0.024 g, 0.365 mmol) were dissolved in acetonitrile (20 mL), and the solution was added to a sample of the

previously prepared ligand solution of the corresponding enantiomer of H2L (5 mL, 0.365 mmol). The mixture was stirred at RT for 3 h, filtered, and layered with diethyl ether. Dark-brown crystals were collected after a week. The analogous reaction starting from MnCl2·4H2O led to complex 6. Elemental analysis calcd (%) for C217H233Br16Mn16N21Na4O49 (1R): C 42.25, H 3.81, N 4.77; found: C 42.0, H 3.6, N 4.4; elemental analysis calcd (%) for C220H234Br16Mn16N24Na4O53 (1S): C 41.86, H 3.74, N 5.33; found: C 41.6, H 3.7, N 4.7. A representative IR spectrum is shown in Figure S4.

Complexes with [Mn4Ca] core (2R, 2S, and 3S): MnCl2·4H2O (0.099 g, 0.5 mmol) and a sample of the previously prepared ligand solution of the corresponding enantiomer of H2L (6 mL, 0.438 mmol) were mixed with Ca(MeO)2 (0.026 g, 0.25 mmol) in acetonitrile (20 mL) and stirred at RT for 3 h. The resulting solution was filtered and layered with diethyl ether. Dark-brown crystals of 2R or 2S were obtained after a few days. The same reaction but starting from MnBr2·4H2O (instead of MnCl2·4H2O) led to complex 3S. Elemental analysis calcd (%) for C100H107.5Ca2Cl10Mn8N7O26.25 (2R): C 44.46, H 4.01, N 3.63; found: C 43.9, H 3.8, N 3.8; elemental analysis calcd (%) for C103.5H113Ca2Cl10Mn8N9O25.5 (2S): C 44.95, H 4.12, N 4.56; found: C 44.3, H 3.9, N 4.3; elemental analysis calcd (%) for C103H109.5Br10Mn8N9O25.25 (3S): C 38.71, H 3.45, N 3.94; found: C 37.4, H 3.7, N 4.1. A representative IR spectrum is shown in Figure S4.

Complexes with [Mn5] core (4R, 4S, and 5S): The same procedure described for complexes 2 and 3 but employing KOH or CsOH (2 mmol) as base led to 4R, 4S, or 5S. Elemental analysis calcd (%) for C101H104Cl10Mn10N8O23 (4R): C 43.90, H 3.88, N 4.15; found: C 42.5, H 4.0, N 4.0; elemental analysis calcd (%) for C105.5H115Cl10Mn10N9O24.5 (4S): C 45.17, H 4.13, N 4.49; found: C 44.1, H 3.8, N 4.3; elemental analysis calcd (%) for C107H116Br10Mn10N8O24.75 (5S): C 39.10, H 3.56, N 4.26; found: C 40.5, H 4.0, N 4.6. A representative IR spectrum is shown in Figure S4.

Complexes with [Mn7Na2] core (6R, 6S, and 7R): MnCl2·4H2O (0.072 g, 0.365 mmol) and NaOH (0.015 g, 0.365 mmol) were stirred for 5 min in acetonitrile (20 mL). After that, a sample of the H2L ligand solution (5 mL, 0.365 mmol) was added. The resulting mixture was stirred at RT for 3 h and filtered. The resulting solution was layered with diethyl ether, and dark-brown crystals were obtained after a few days. The same reaction but starting from MnBr2·4H2O (instead of MnCl2·4H2O) led to complex 7R. Elemental analysis calcd (%) for C105H111Cl6Mn7N6Na2O23 (6R): C 50.24, H 4.46, N 5.02; found: C 50.5, H 4.1, N 4.8; elemental analysis calcd (%) for C97.5H100Cl6Mn7N6Na2O23.5 (6S): C 49.30, H 4.24, N 3.54; found: C 49.4, H 3.7, N 3.7; elemental analysis calcd (%) for C108H112Br6Mn7N10Na2O21 (7R): C 46.03, H 3.94, N 4.13; found: C 45.8, H 3.8, N 4.3. A representative IR spectrum is shown in Figure S4

Conflict of interest

The authors declare no conflict of interest.

601

602

603　[1]　a) R. Sessoli, D. Gatteschi, A. Caneschi, M. Novak, Nature 1993, 365, 141–143; b) J. Villain, F.
604　　　　Hartman-Benton, R. Sessoli, A. Rattori, Europhys. Lett. 1994, 27, 159–164.

605　[2]　a) E. S. Koumousi, S. Mukherjee, C. M. Beavers, S. J. Teat, G. Christou, T. C. Stamatatos,
606　　　　Chem. Commun. 2011, 47, 11128–11130; b) D. R. J. Kolling, N. Cox, G. M. Ananyev, R. J.
607　　　　Pace, G. C. Dismukes, Biophys. J. 2012, 103, 313–322; c) C. Zhang, C. Chen, H. Dong, J.-R.
608　　　　Shen, H. Dau, J. A. Zhao, Science 2015, 348, 690–693.

609　[3]　I. J. Hewitt, J.-K. Tang, N. T. Madhu, R. Clerac, G. Buth, C. E. Anson, A. K. Powell, Chem.
610　　　　Commun. 2006, 2650–2652.

611　[4]　L.-L. Fan, F.-S. Guo, L. Yun, Z.-J. Lin, R. Herchel, J.-D. Leng, Y.-C. Ou, M.-L. Tong, Dalton
612　　　　Trans. 2010, 39, 1771–1780.

613　[5]　S. Nayak, H. P. Nayek, S. Dehnen, A. K. Powell, J. Reedijk, Dalton Trans. 2011, 40, 2699–
614　　　　2702.

615　[6]　P.-P. Yang, C.-Y. Shao, L.-L. Zhu, Y. Xu, Eur. J. Inorg. Chem. 2013, 5288 –5296.

616　[7]　P.-P. Yang, L.-L. Zhu, Y. Xu, C.-Y. Shao, Z. Anorg. Allg. Chem. 2013, 639, 1821–1826.

617　[8]　C. Ding, C. Gao, S. Ng, B. Wang, Y. Xie, Chem. Eur. J. 2013, 19, 9961 – 9972.

618　[9]　L. Cong, X. Qin, W. Sun, Y. Wang, S. Ding, Z. Liu, New J. Chem. 2014, 38, 545–551.

619　[10]　Y. Song, G. Zhang, X. Qin, Y. Gao, S. Ding, Y. Wang, C. Du, Z. Liu, Dalton Trans. 2014, 43,
620　　　　3880–3887.

621　[11]　a) V. Chandrasekhar, A. Dey, S. Das, S. Kundu, CrystEngComm 2014, 16, 1304–1310; b) P.-P.
622　　　　Yang, X.-L. Wang, L.-C. Li, D.-Z. Liao, Dalton Trans. 2011, 40, 4155–4161.

623　[12]　D. Liu, Q. Zhou, Y. Chen, F. Yang, Y. Yu, Z. Shi, S. Feng, Dalton Trans. 2010, 39, 5504–5508.

624　[13]　a) A. Escuer, J. Mayans, M. Font-Bardia, L. Di Bari, M. Gjrecki, Eur. J. Inorg. Chem. 2017,
625　　　　991–998; b) A. Escuer, J. Mayans, M. Font-Bardia, M. Gjrecki, L. Di Bari, Dalton Trans. 2017,
626　　　　46, 6514–6517; c) J. Mayans, A. Martin, M. Font-Bardia, A. Escuer, Polyhedron 2018, 150, 10–
627　　　　14; d) J. Mayans, M. Font-Bardia, A. Escuer, Inorg. Chem. 2018, 57, 926–929; e) J. Mayans, M.
628　　　　Font-Bardia, A. Escuer, Dalton Trans. 2018, 47, 8392–8401; f) J. Mayans, M. Font-Bardia, L.
629　　　　Di Bari, L. Arrico, F. Zinna, G. Pescitelli, A. Escuer, Chem. Eur. J. 2018, 24, 7653–7663.

630   [14]   A. Escuer, J. Esteban, S. P. Perlepes, T. C. Stamatatos, Coord. Chem. Rev. 2014, 275, 87–129.

631   [15]   a) J. Crassous, Chem. Soc. Rev. 2009, 38, 830–845; b) H. Miyake, Symmetry 2014, 6, 880–895.

632   [16]   a) K. Mikami, M. Lautens, New Frontiers in Asymmetric Catalysis, Wiley, Germany, 2007; b) J.
633   Kumar, T. Nakashima, T. Kawai, J. Phys. Chem. Lett. 2015, 6, 3445–3452.

634   [17]   a) S. Muhlbauer, B. Binz, F. Jonietz, C. Pfleiderer, A. Rosch, A. Neubauer, R. Georgii, P. Boni,
635   Science 2009, 323, 915–919; b) X. Z. Yu, Y. Onose, N. Kanazawa, J. H. Park, J. H. Han, N.
636   Nagaosa, Y. Tokura, Nature 2010, 465, 901–904; c) Y. Togawa, T. Koyama, K. Takayanagi, S.
637   Mori, Y. Kousaka, J. Akimitsu, S. Nishihara, K. Inoue, A. S. Ovchinnikov, J. Kishine, Phys.
638   Rev. Lett. 2012, 108, 107202.

639   [18]   a) S.-Y. -Lin, Y.-N. Guo, L. Zhao, P. Zhang, H. Ke, Chem. Commun. 2012, 48, 6924–6926; b)
640   S.-Y- Lin, C. Wang, L. Zhao, J. Tang, Chem. Asian J. 2014, 9, 3558–3564; c) S.-Y. Lin, C.
641   Wang, L. Zhao, J. Wu, J. Tang, Dalton Trans. 2015, 44, 223.

642   [19]   J.-C. G. Benzli, S. V. Eliseeva, Chem. Sci. 2013, 4, 1939–1949.

643   [20]   M. Liu, L. Zhang, T. Wang, Chem. Rev. 2015, 115, 7304–7397.

644   [21]   a) M. Viciano-Chumillas, S. Tanase, I. Mutikainen, U. Turpeinen, L. J. de Jongh, J. Reedijk,
645   Inorg. Chem. 2008, 47, 5919–5929; b) T. C. Stamatatos, D. Foguet-Albiol, S. C. Lee, C. C.
646   Stoumpos, C. P. Raptopoulou, A. Terzis, W. Wernsdorfer, S. O. Hill, S. P. Perlepes, G.
647   Christou, J. Am. Chem. Soc. 2007, 129, 9484–9499; c) J. Cano, T. Cauchy, E. Ruiz, C. J.
648   Milios, C. C. Stoumpos, T. C. Stamatatos, S. P. Perlepes, G. Christou, E. K. Brechin, Dalton
649   Trans. 2008, 234–240.

650   [22]   C. Lampropoulos, K. A. Abboud, T. C. Stamatatos, G. Christou, Inorg. Chem. 2009, 48, 813–
651   815.

652   [23]   N. F. Chilton, R. P. Anderson, L. D. Turner, A. Soncini, K. S. Murray, J. Comput. Chem. 2013,
653   34, 1164–1165.

654   [24]   G. M. Sheldrick, SHELXL-2014/7: Program for the Solution of Crystal Structures, University of
655   Gçttingen, Gçttingen, Germany, 2014.

656   [25]   L. J. Farrugia, J. Appl. Crystallogr. 1997, 30, 565.

657

Legends to figures

659

660   **Scheme 1.** Arrangement of the ligands in pentanuclear cages based on the Schiff bases obtained by

661   condensation of o-vanillin and 3-amino-1,2-propanediol (I, literature data) or 2-amino-1-ethanol (II and

662   III, this work). See Figure 1 for the color key.

663

664   **Scheme 2.** H2L Schiff bases employed in this work (top), and their coordination modes linking three

665   cations (bottom). The asterisk denotes the chiral C atom.

666

667   **Figure. 1**. A view of the 1RA molecule and its labeled core (top). Tetra-, penta-, and hexacoordinate

668   environments for the divalent Mn4 cation (bottom). Color key for all figures: MnIII dark green; MnII

669   orange; CaII forest green; NaI blue; Cl violet; Br firebrick; O red; N navy; C dark gray.

670

671   **Figure. 2**. A view of the representative 2RA molecule (left) and its labelled core (right).

672

673   **Figure. 3** A view of the representative 4RA molecule (left) and its labelled core (right).

674

675   **Figure. 4** A view of the representative 6R molecule (top) and its labeled core

676   (bottom).

677

678   **Figure. 5** Space-fill view of complex 1 showing the opposite helicity for 1R and 1S (top). Arrangement

679   of the bidentate fragments around the NaI cations (bottom). Fragments depicted as red rings turn D, and

680   fragments depicted as green rings turn L. Left, R enantiomer; right, S enantiomer.

681

682   **Figure. 6** Plot of the coordination of the O donors around the CaII cations and the ideal apicated

683   octahedron polyhedron for complexes 2–5. The bidentate fragments show two mirror images of opposite

684   helicities around the cation. Fragments depicted as red rings turn D, and fragments depicted as green

685   rings turn L.

686

687   **Figure. 7** Trigonal rotation of the central MnII coordination sphere (top) that determines a L or D

688   conformation (bottom) for 6R (left) and 6S (right), respectively.

689

690   **Scheme 3**. Reaction scheme showing the conditions that lead to four different systems from the H2L

691   ligand.

692

693   **Figure. 8** ECD spectra for the pairs of enantiomers of complexes 1 (top), 2 (middle), and 6 (bottom).

694   (R)-enantiomers, red lines; (S)-enantiomers, blue lines. The spectrum of 4R (green line) appears to be

695   identical to that of 2R.

696

697   **Scheme 4.** Key for the structural parameters summarized in Table 5.

698

699   **Scheme 5.** Coupling scheme for complexes 1 (top, left), 2 and 3 (top, middle), 4 and 5 (top, right), and 6

700   and 7 (bottom).

701

702   **Figure. 9** cMT versus T and magnetization (inset) plots for complex 1S. Solid lines show the fit of the

703   experimental data.

704

705   **Figure. 10** cMT versus T and magnetization (inset) plots for complexes 2R (squares), 3S (triangles), 4R

706   (circles), and 5S (diamonds). Solid lines show the fit of the experimental data.

707

708   **Figure. 11** cMT versus T plots for complexes 6R (circles) and 7R (diamonds). Solid lines show the fit

709   of the experimental data.

710

711   **Figure. 12** Evolution of the ground state for the MnIIMnIII6NaI2 system versus the intertriangle

712   interaction, in relation to the 19/2 spin state (top). Effect on the cMT and M response of the intertriangle

713   interaction (bottom).

714

715
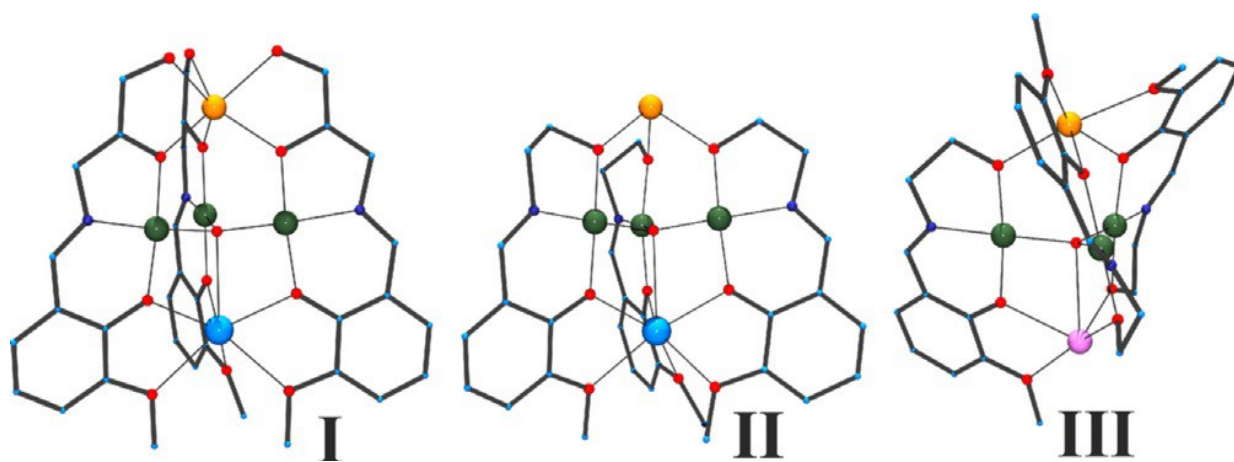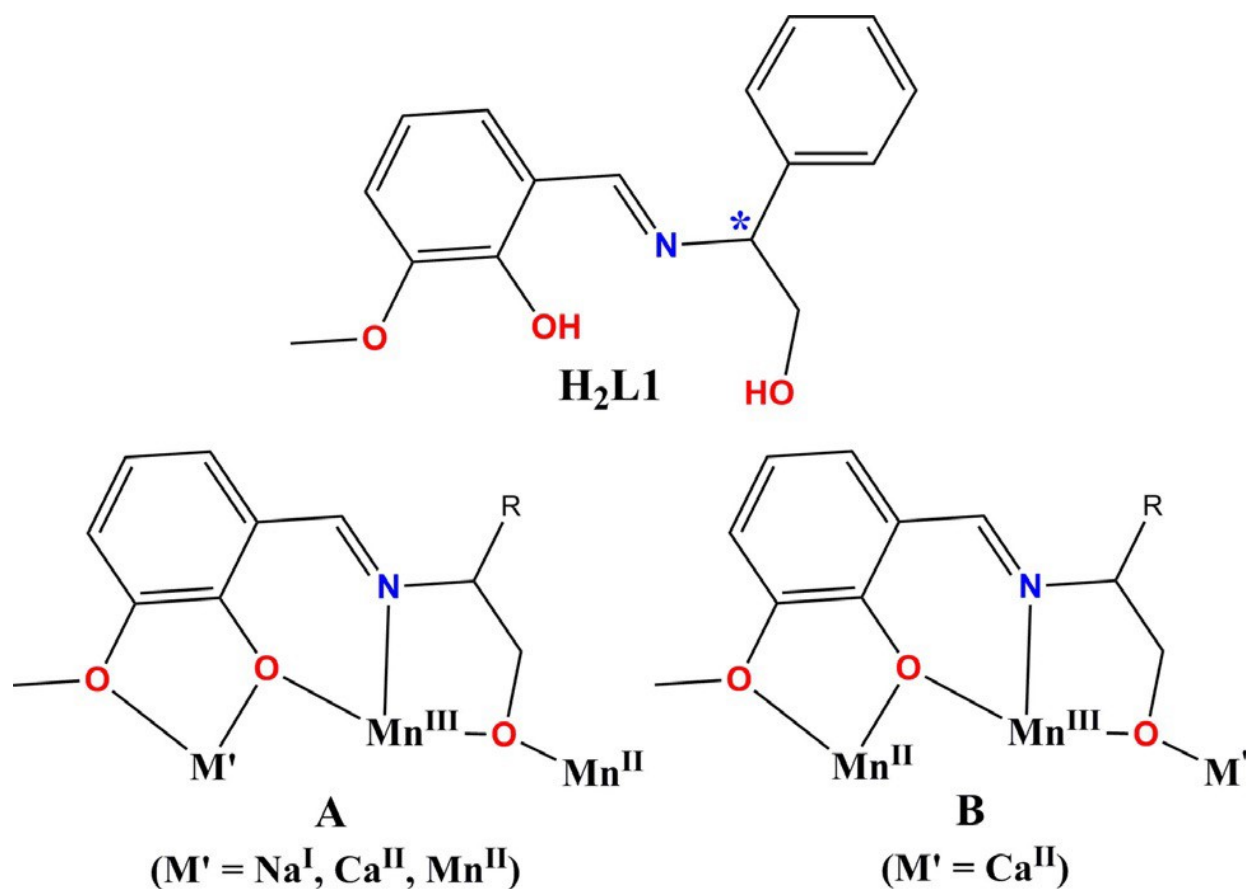
Scheme 1.

I **II** **III**

.

SCHEME 2.

H_2L1

A
(M' = Na^I, Ca^{II}, Mn^{II})

B
(M' = Ca^{II})
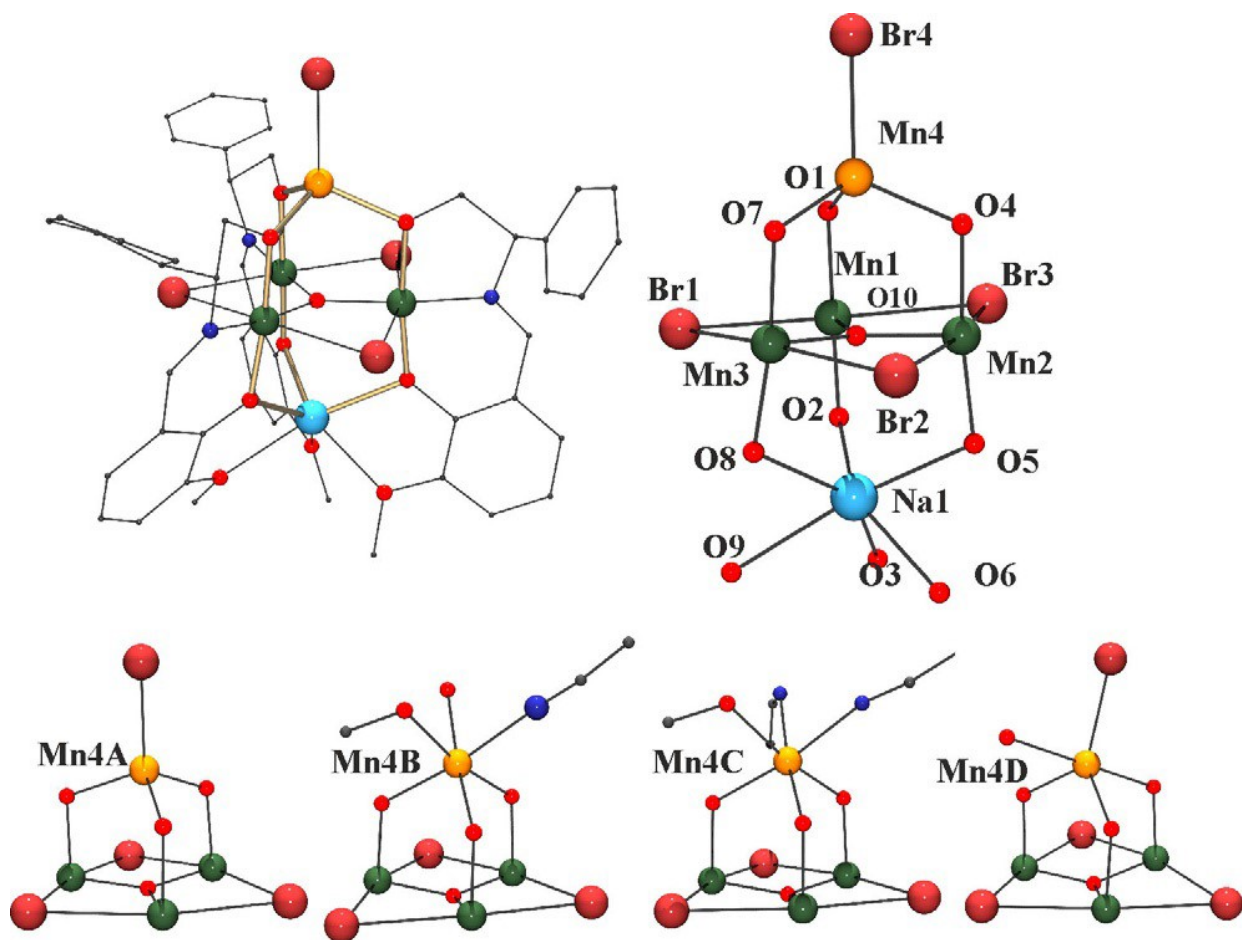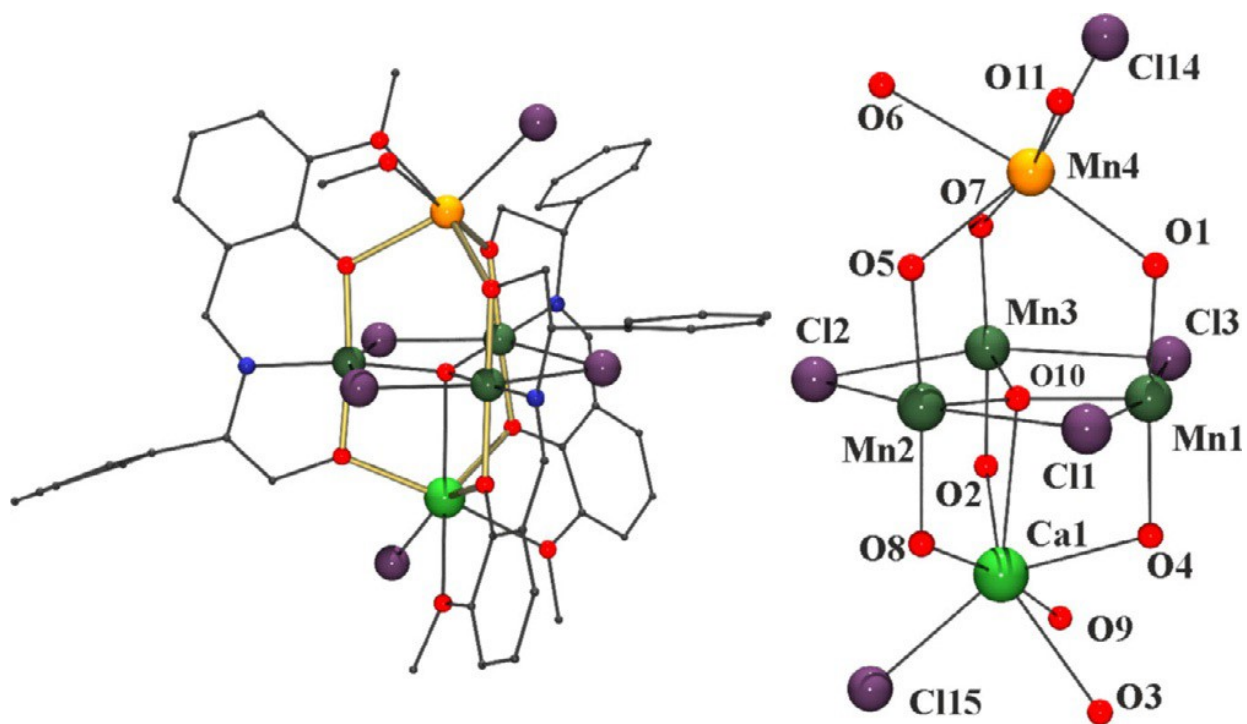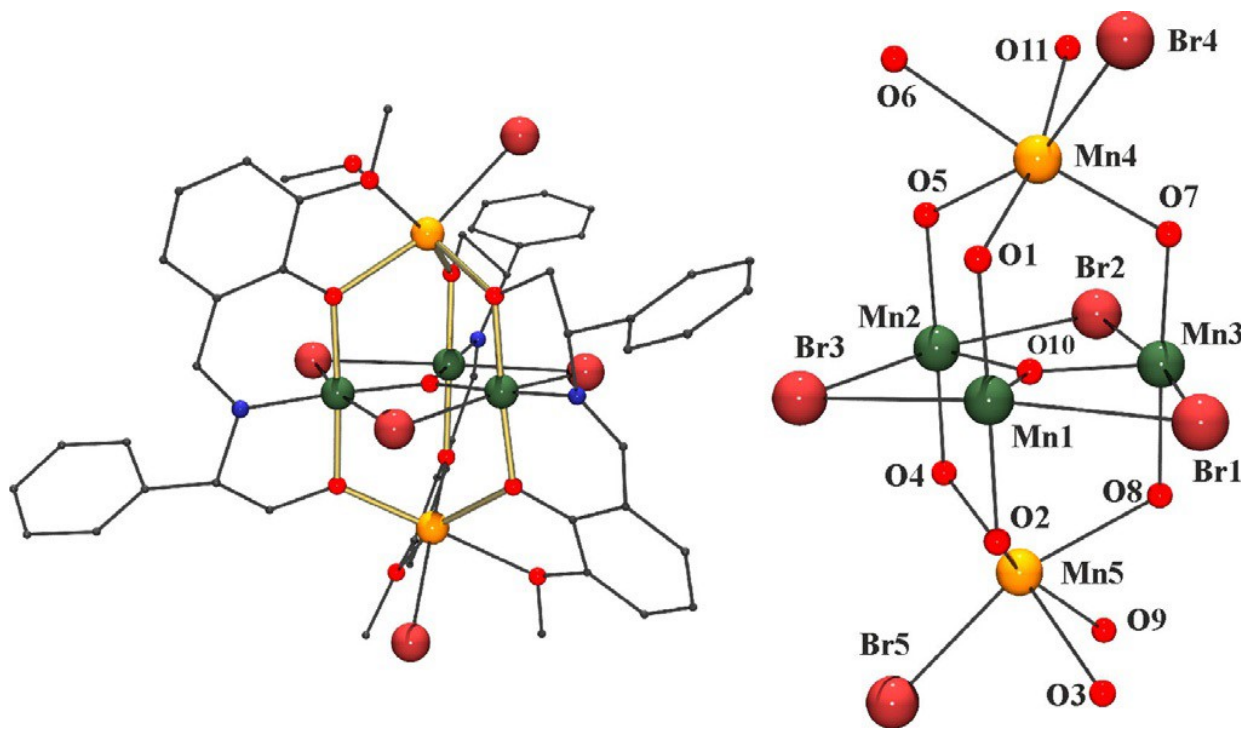
FIGURE 1

FIGURE 2

FIGURE 3

FIGURE 4

745

746

747

748

749

750

751

752

753

754
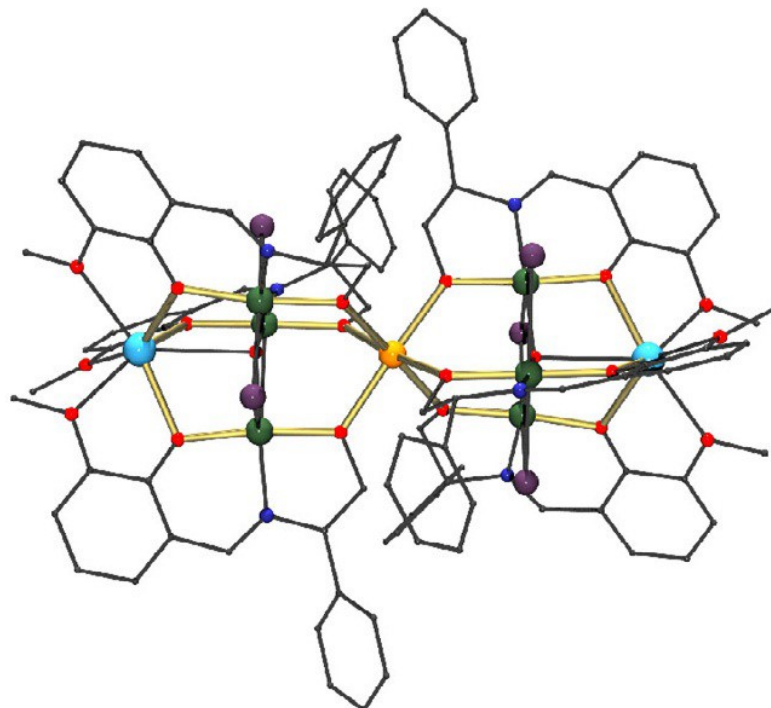
755

756

757

758

759

760

761

762

763

764
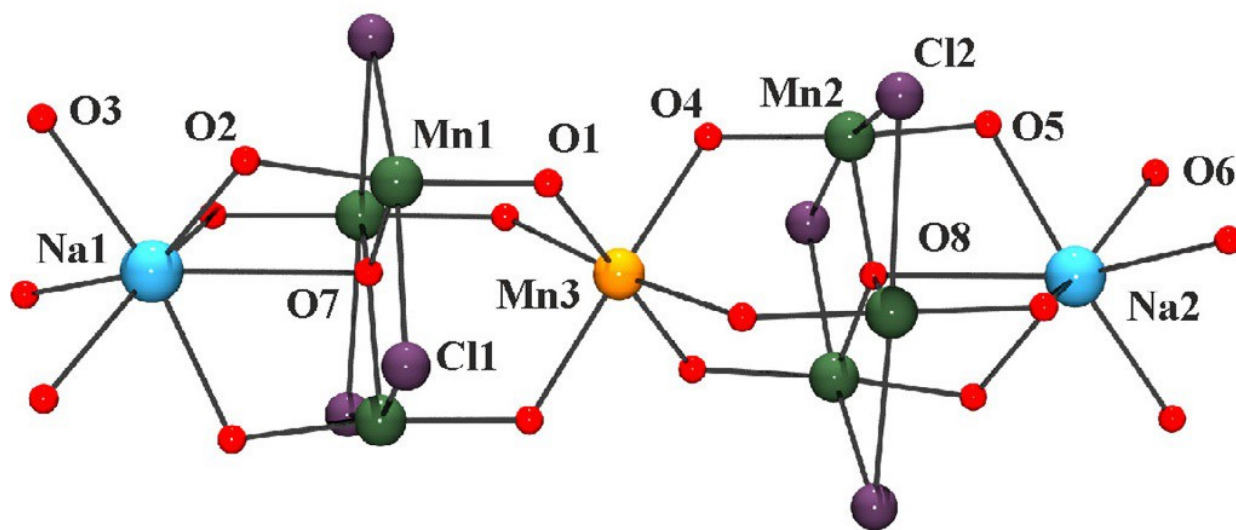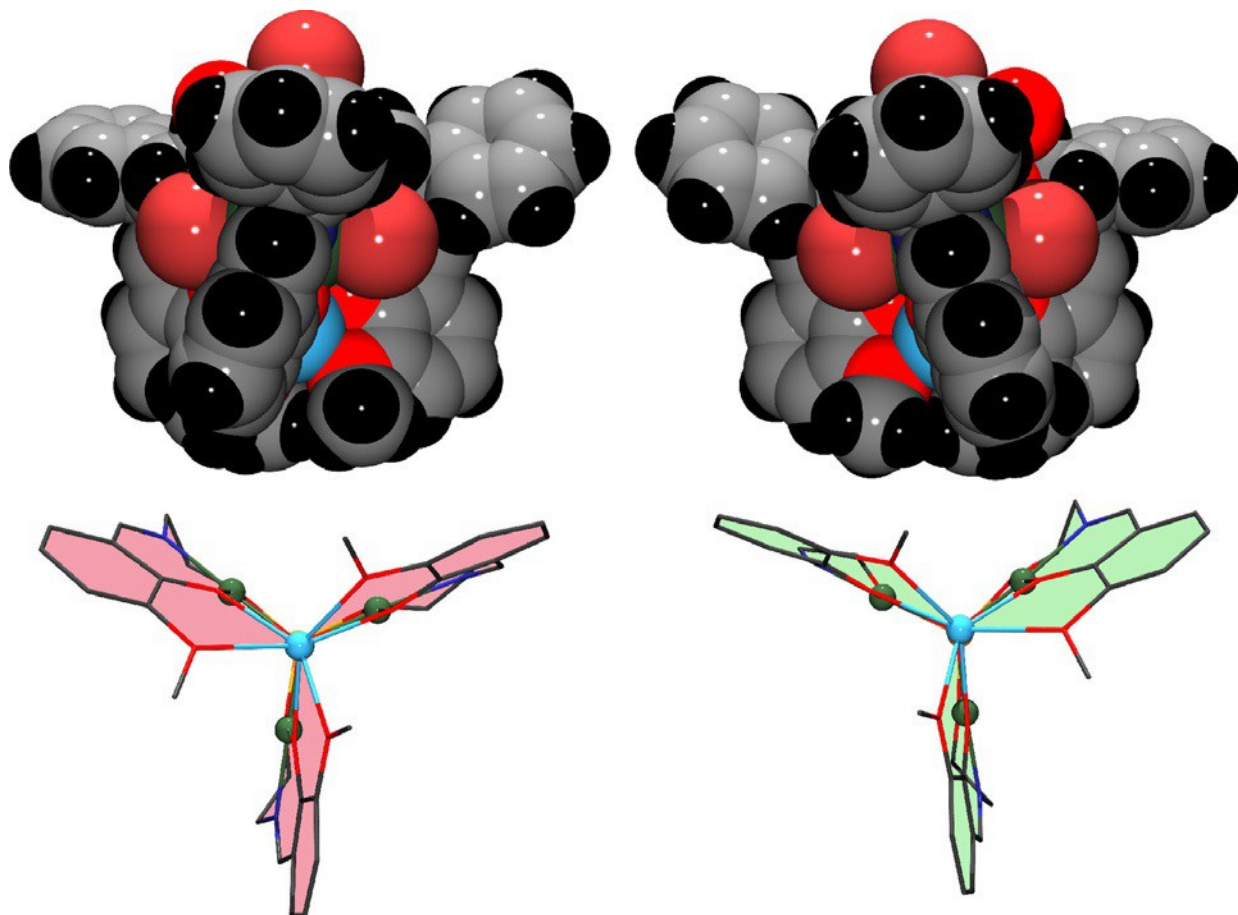
FIGURE 5.

771   **FIGURE 6.**

772

773
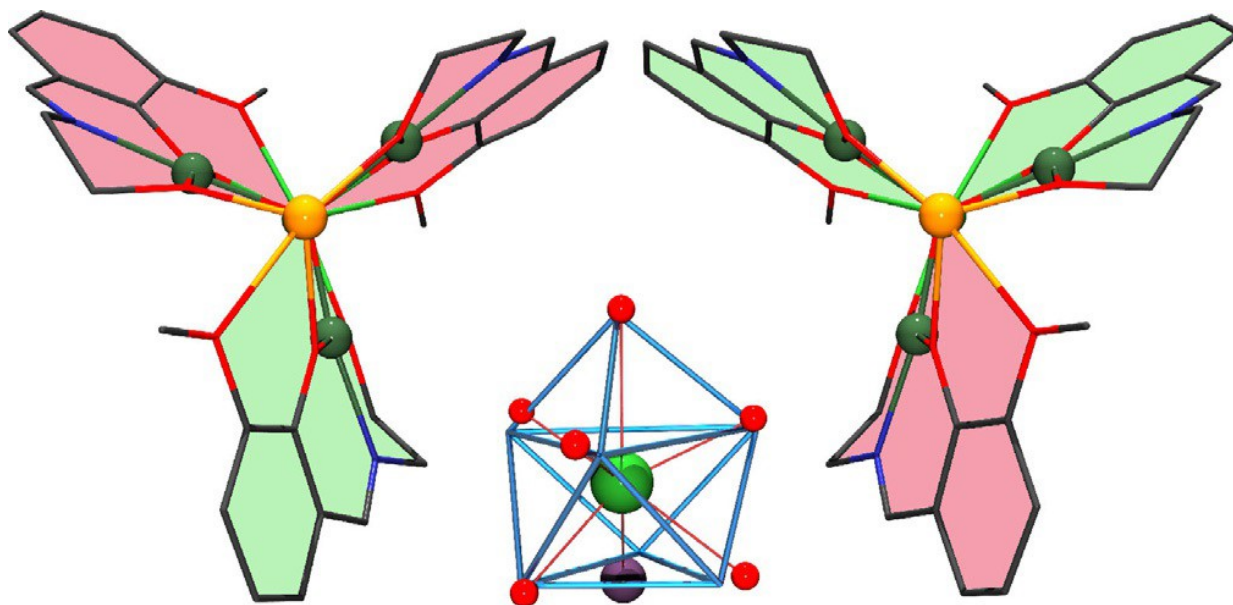
774

775
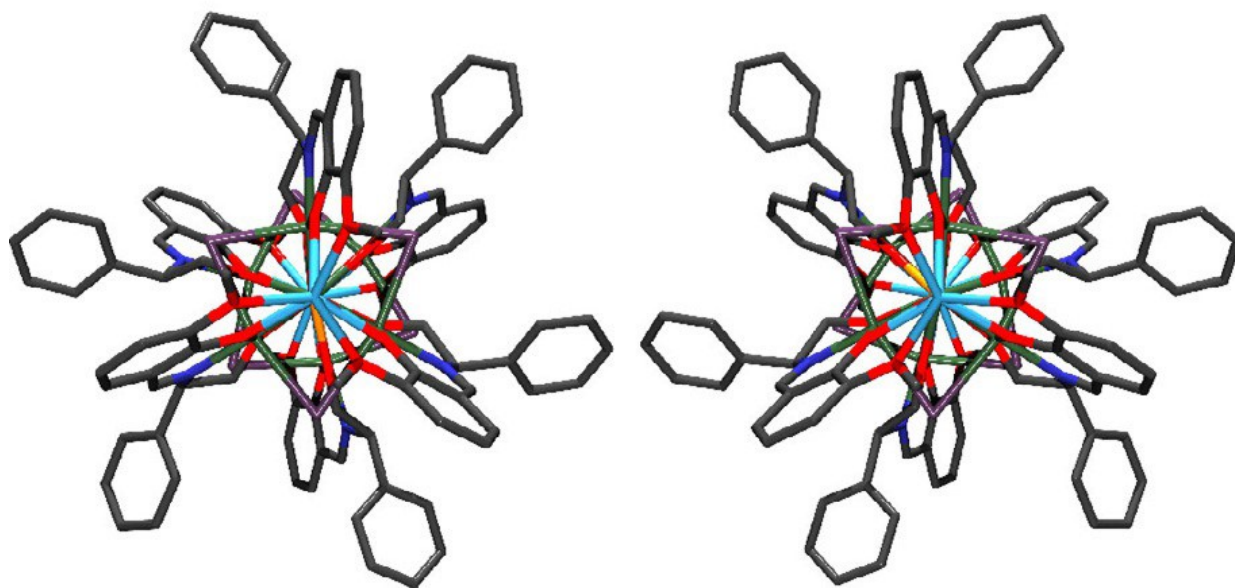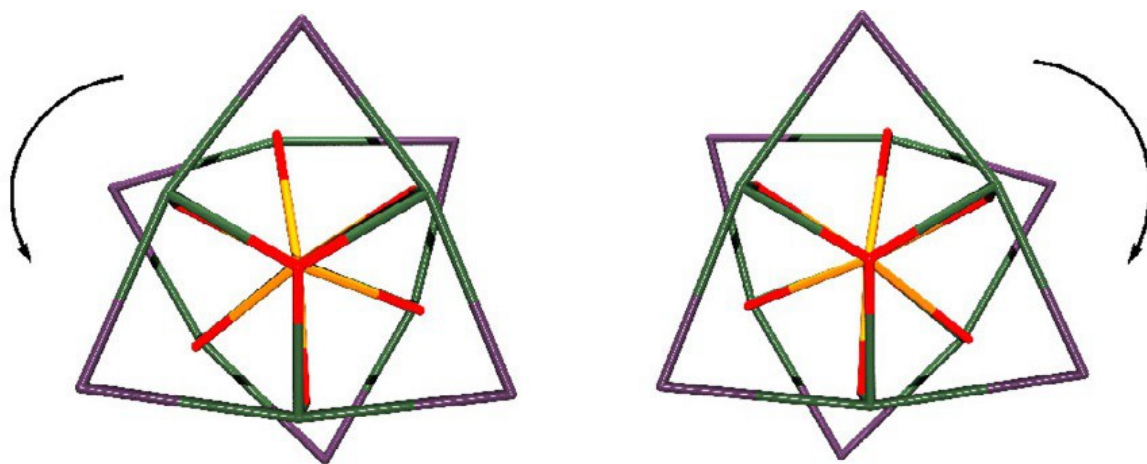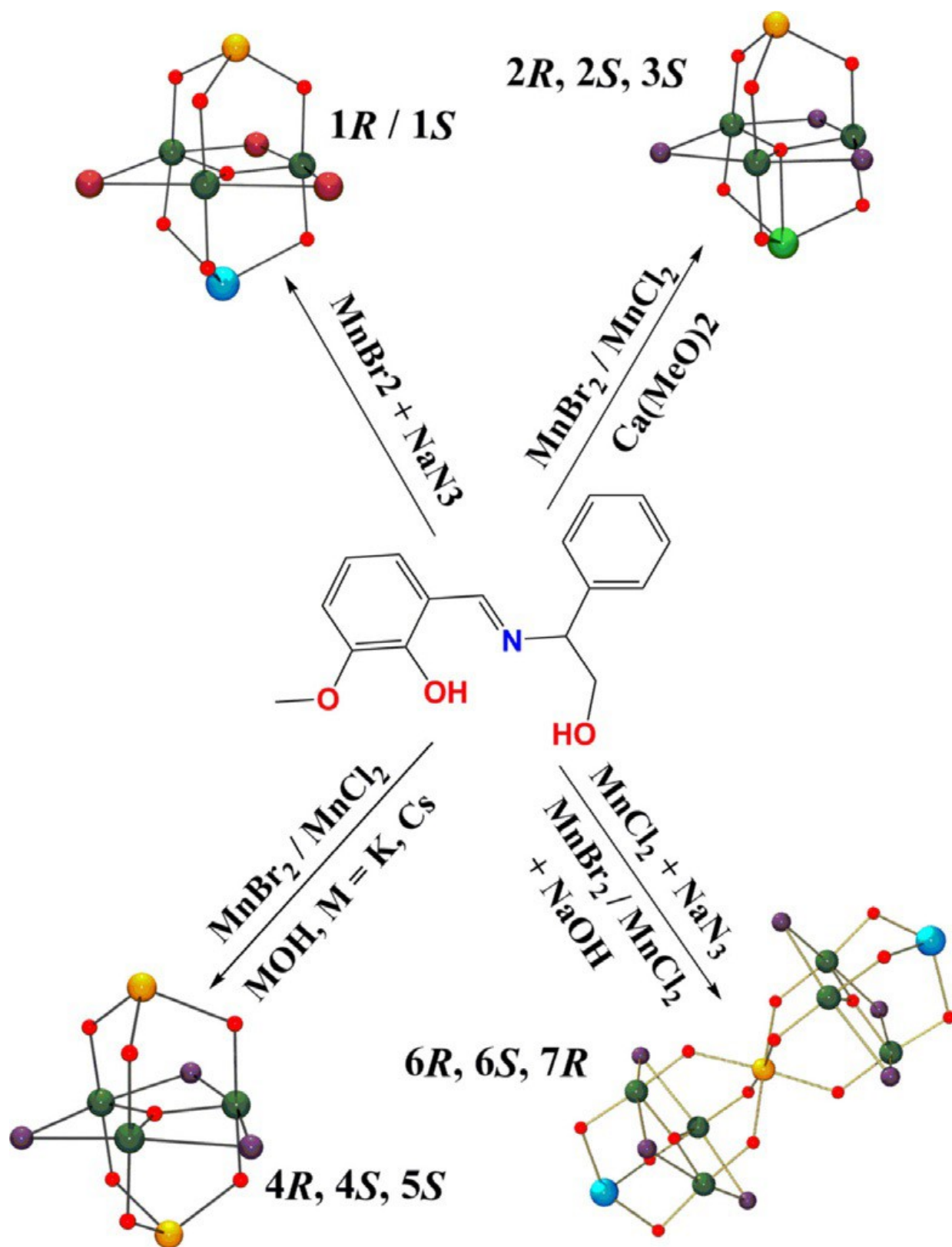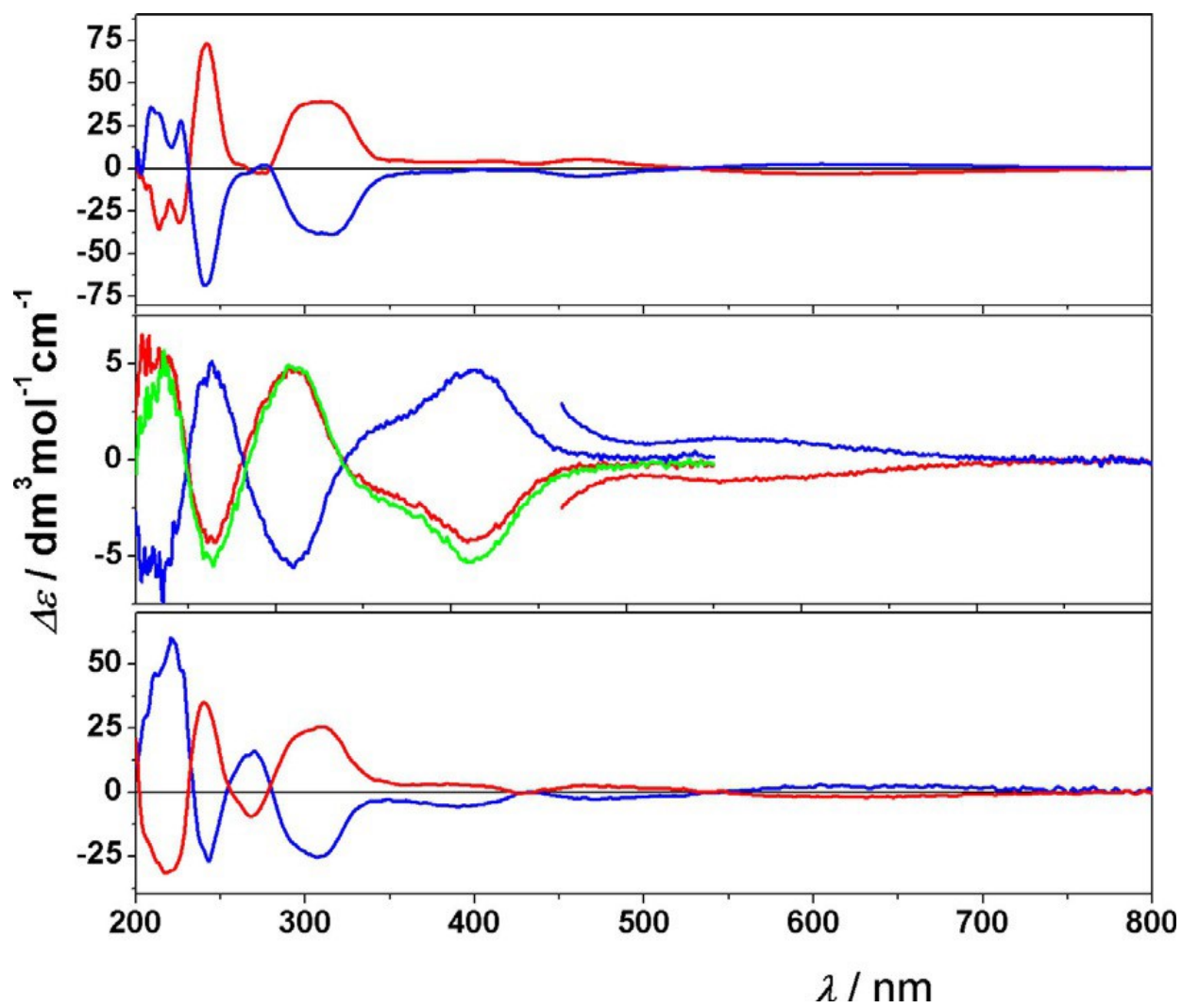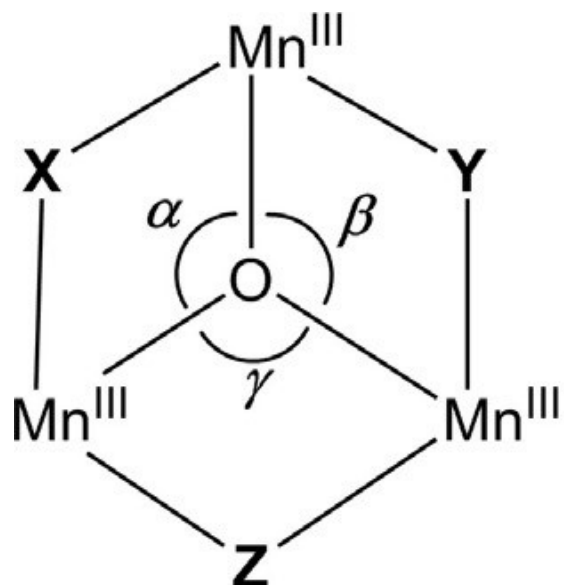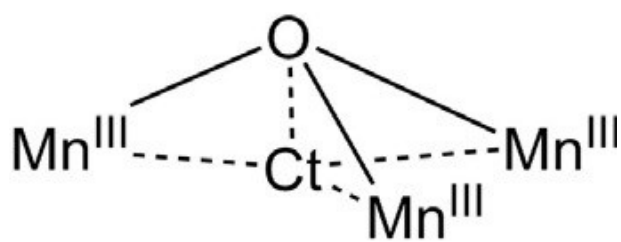
FIGURE 7.

SCHEME 3.

FIGURE 8.

SCHEME 4.

SCHEME 5.
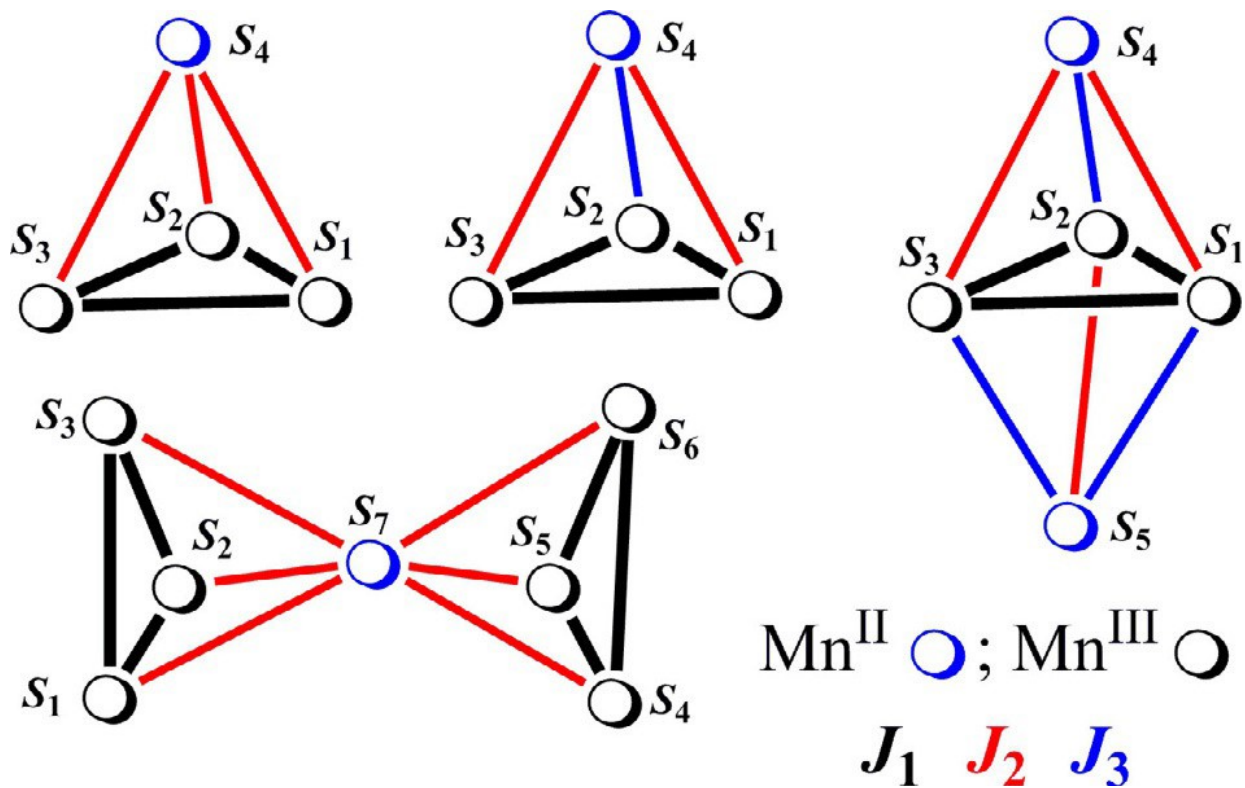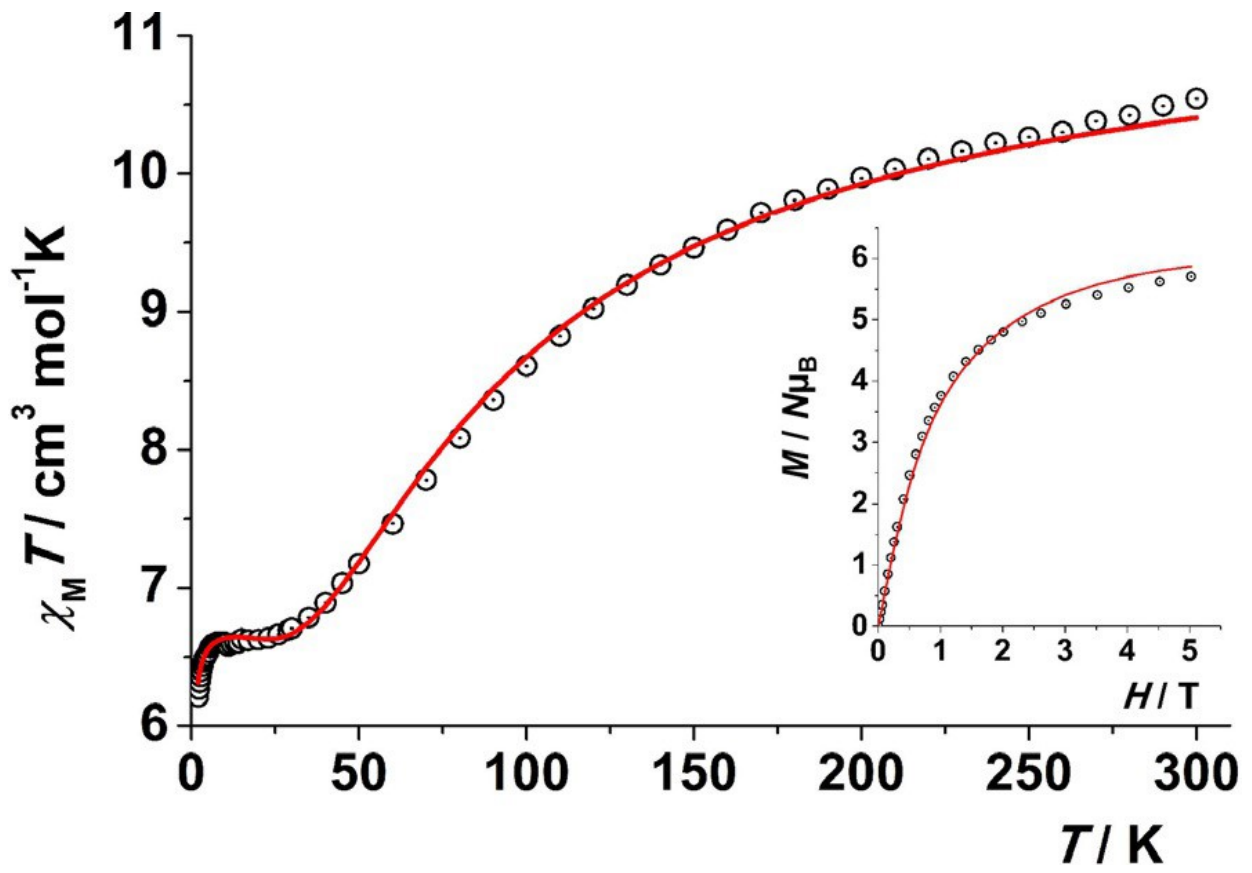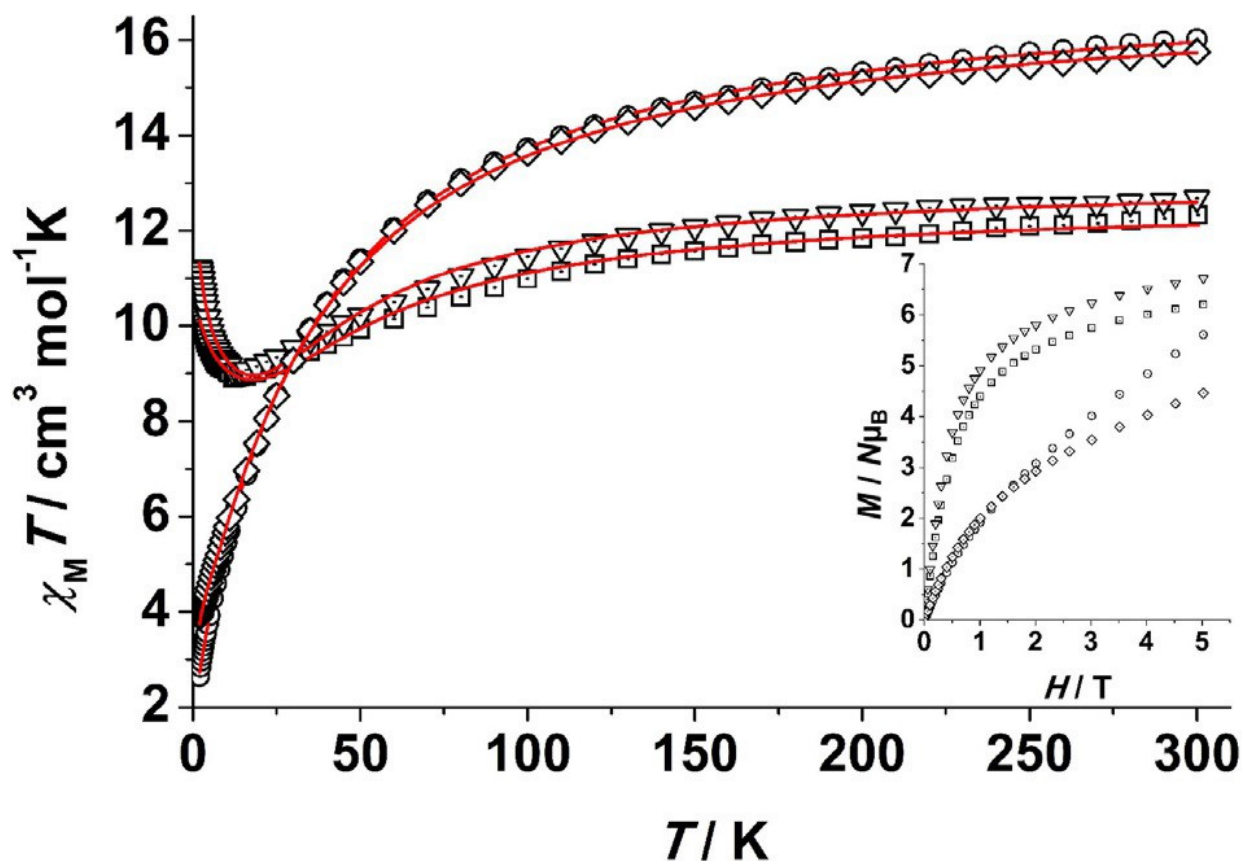
FIGURE 9.

FIGURE 10.

FIGURE 11.
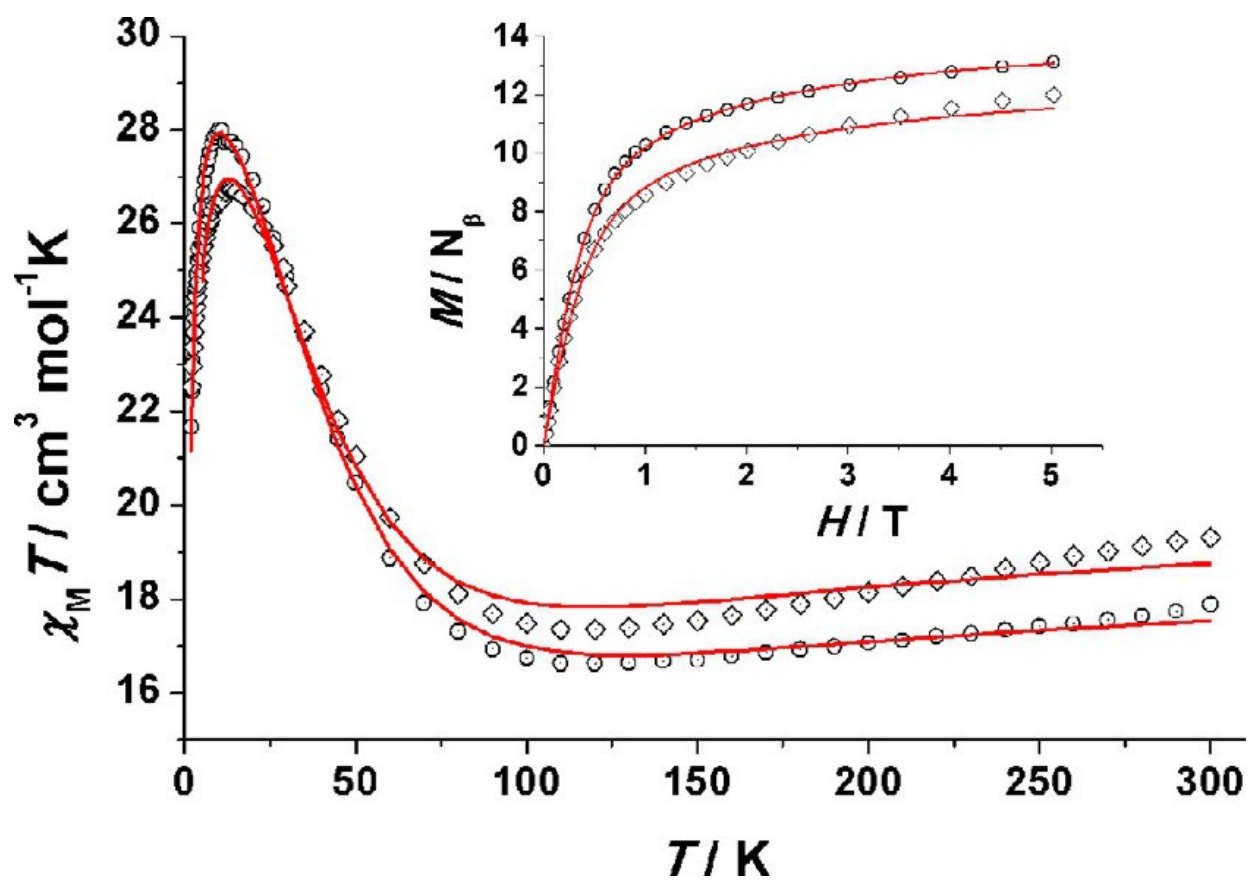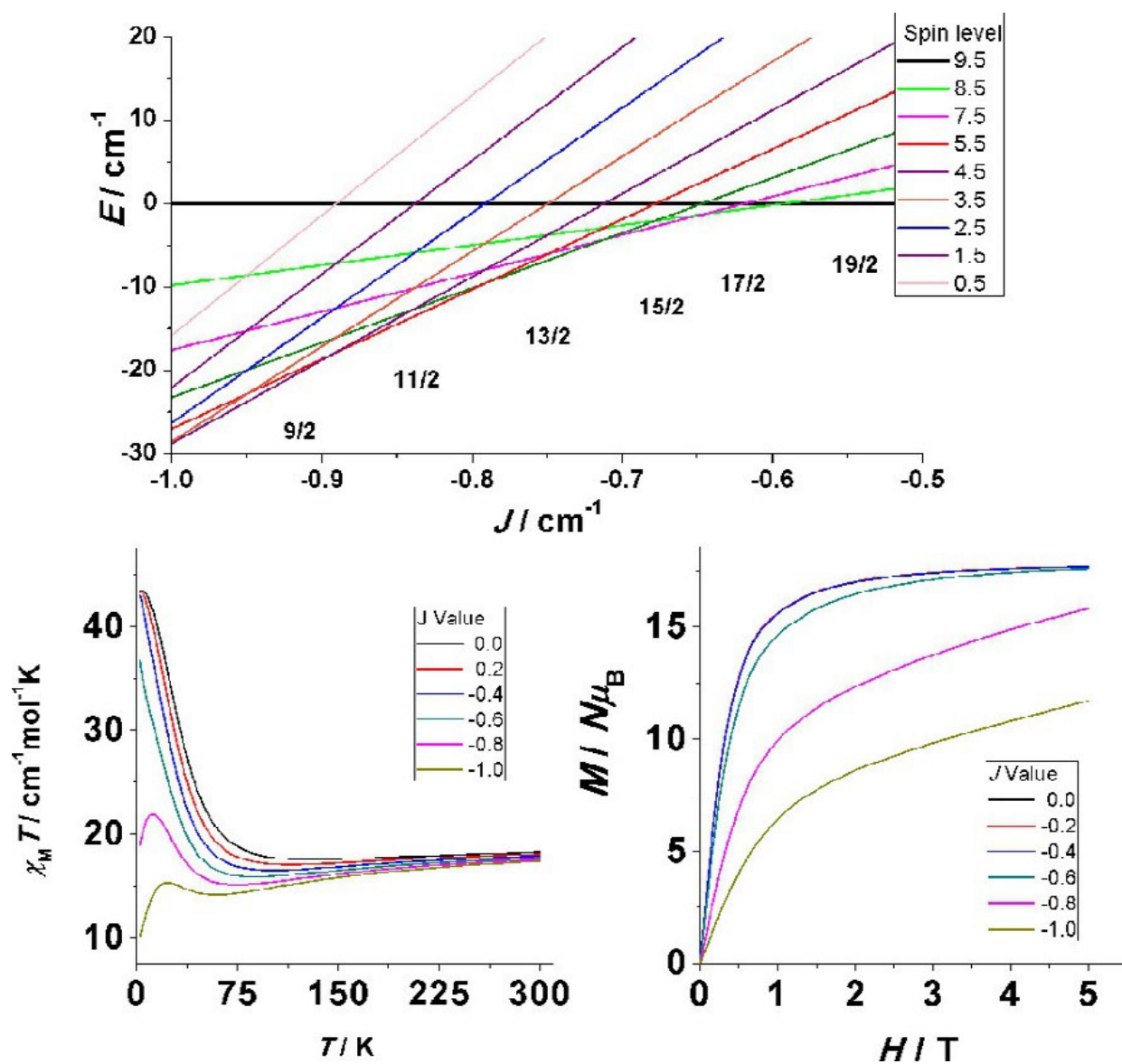
826   **FIGURE 12.**

827

828

829

830